



Marshallplan-Jubiläumsstiftung  
Austrian Marshall Plan Foundation

MARSHALL PLAN SCHOLARSHIP FINAL REPORT

# Influence of the polycystin-1 C-terminal fragments on mitochondrial function in polycystic kidney disease

Hannah Pellegrini

BACHELOR DEGREE COURSE

BIOTECHNOLOGY

31.07.2017

# Acknowledgement

Foremost, I would like to express my sincere gratitude to the Austrian Marshall Plan Foundation for their Marshall Plan Scholarship as a financial support, without which this research stay would not have been possible.

My sincere thanks goes to my supervisor Thomas Weimbs, PhD for accepting me to conduct research in his lab at the University of California, Santa Barbara. His guidance helped me in all the time of my project and writing of this thesis and I would like to thank him for his patience, motivation, enthusiasm, and immense knowledge from which I very much benefitted. Besides my supervisor, I would like to thank the other members of the Weimbs lab for their help and encouragement.

Further, I want to thank the Management Center Innsbruck as my home institution for all the support and collaboration. I thank my advisor and head of the study program Biotechnology FH-Prof. Dr. Christoph Griesbeck for his support and taking the time to review this bachelor's thesis.

# Abstract

Autosomal dominant polycystic kidney disease is the most common life-threatening monogenic inherited disease. The loss of functional polycystin-1 signaling encoded by the PKD1 gene causes renal cyst growth eventually resulting in kidney failure. Disease progression results in an oxygen deficiency affecting cyst lining cells. In ADPKD, the C-terminal cytoplasmic tail of polycystin-1 is cleaved and yields the protein fragment PC1-p30 which contains the shorter fragment PC1-p15. PC1-p15 constitutively targets mitochondria whereas the mitochondrial targeting signal of PC1-p30 is unmasked under hypoxic conditions. The accumulation of the protein fragments in mitochondria is associated with morphological alterations and a metabolic shift similar to the Warburg-effect observed in cancer cells, enabling the cyst lining cells to survive under hypoxic conditions. The Warburg metabolism is characterized by energy conversion through aerobic glycolysis rather than aerobic respiration, even under normoxic conditions. It was tested whether and how the C-terminal fragments impair mitochondrial function and promote the Warburg-like metabolic shift. The findings tentatively indicate that the expression of the protein fragments entail similar effects on mitochondria as observed in cancer cells exhibiting the Warburg effect and may constitute a protection mechanism promoting disease progression.

# Contents

<b>1</b>	<b>Introduction</b>	<b>1</b>
<b>2</b>	<b>Research Background</b>	<b>2</b>
<b>3</b>	<b>Experiments</b>	<b>7</b>
3.1	Limitations . . . . .	7
3.2	Cell Line . . . . .	8
3.3	Mitochondrial Membrane Potential (MMP, $\Delta\Psi_m$ ) . . . . .	9
3.4	Reactive Oxygen Species (ROS) . . . . .	9
3.5	Proliferation, Cell Survival, Apoptosis and Necrosis . . . . .	10
3.6	Data Acquisition: Flow Cytometry . . . . .	10
<b>4</b>	<b>Methods</b>	<b>12</b>
4.1	Cell Culture . . . . .	12
4.2	Mitochondrial Membrane Potential (MMP, $\Delta\Psi_m$ ) assay . . . . .	13
4.3	Superoxide detection assay . . . . .	17
4.4	Growth Curve and Cell Permeabilization detection assay . . . . .	19
<b>5</b>	<b>Results</b>	<b>22</b>
5.1	Mitochondrial Membrane Potential . . . . .	22
5.2	Superoxide production . . . . .	24
5.3	Proliferation, Cell Survival, Apoptosis and Necrosis . . . . .	25
5.3.1	MDCK-p30 cells cultured in standard glucose concentration . . . . .	25
5.3.2	MDCK-p30 cells cultured in low glucose concentration . . . . .	26
5.3.3	MDCK-p15 cells cultured in standard glucose concentration . . . . .	27
5.3.4	MDCK-p15 cells cultured in low glucose concentration . . . . .	28
<b>6</b>	<b>Discussion</b>	<b>29</b>
6.1	Mitochondrial Membrane Potential . . . . .	30

6.2	Superoxide production . . . . .	31
6.3	Proliferation, Cell Survival, Apoptosis and Necrosis . . . . .	32
<b>7</b>	<b>Conclusion</b>	<b>34</b>
<b>8</b>	<b>Future Outlook</b>	<b>35</b>
	<b>References</b>	<b>iii</b>
	<b>List of Figures</b>	<b>xiii</b>
	<b>List of Tables</b>	<b>xv</b>
	<b>List of Symbols</b>	<b>xvi</b>
	<b>Appendix</b>	<b>xvii</b>

# 1 Introduction

Affecting more than 600,000 people in the US alone and millions of people worldwide, autosomal dominant polycystic kidney disease (ADPKD) is one of the most common life-threatening, monogenic inherited diseases. The growing renal cysts are small, fluid filled sacs which can develop at a young age, but often remain undiagnosed until reaching mid-life, when pathogenic symptoms arise. Although some of these symptoms can be treated, there is currently no cure for ADPKD [1, 2]. Moreover, ADPKD can lead to other potentially serious problems such as high blood pressure, which then again increases the risk of heart attacks and strokes [3]. For patients with progressed disease, nothing but life-long kidney dialysis or kidney transplantation remains to ensure survival [4].

Autosomal dominant polycystic kidney disease (ADPKD) is induced by the loss of functional copies of either the protein polycystin-1 (PC1) or polycystin-2 (PC2), causing renal cyst growth which eventually results in progressive kidney failure [5]. Due to the cyst growth, the kidney structure changes dramatically and oxygen supply becomes limited in cyst-lining cells [6]. While normal kidney cells are not able to survive in a low-oxygen environment, cyst cells somehow remain capable of proliferation due to a change in their metabolism. This metabolic shift is associated with an increased level of a small protein fragment (PC1-p30), accumulating in cyst-lining cells under hypoxic conditions. PC1-p30 is cleaved from PC1 in ADPKD, targets mitochondria under hypoxia and in a mechanism not known, changes the shape and function of mitochondria, the energy-converting organelle which normally uses oxygen to perform this task. Further, another defined fragment corresponding to half of the cytoplasmic tail (PC1-p15) is overexpressed in ADPKD kidneys and constitutively targets mitochondria possibly playing another or similar disease-promoting role. Investigating how the two fragments influence mitochondrial function and therefore help cyst cells to survive in low-oxygen environments was the main aim of this research project.

## 2 Research Background

Mutations in either the gene PKD1 or PKD2 are the underlying cause of ADPKD, whereby mutations in PKD1 account for 85% of the cases and PKD2 for 15%, both encoding for the proteins polycystin-1 (PC1) or polycystin-2 (PC2) respectively. Currently, the natural function of PC1 and PC2 is poorly understood and it is still unclear why these mutations lead to renal cyst growth. It is known that both PC1 and PC2 are large transmembrane proteins which form a complex and that PC1 interacts with many signaling proteins. It also regulates several signaling pathways [7, 8]. PC2 is a  $\text{Ca}^{2+}$ -permeable ion channel [9] that is located to the plasma membrane and to intracellular compartments where it can regulate  $\text{Ca}^{2+}$ -release from the endoplasmic reticulum [10]. Further, the PC complex also localizes to the primary cilium, possibly being involved in mechano-and chemosensory pathways [11, 12].

PC1 undergoes proteolytic cleavage in ADPKD. Thus, the C-terminal cytoplasmic tail is released from the membrane, yielding the small fragment PC1-p30 (molecular weight  $\sim 30$  kDa). Shown in previous studies, PC1-p30 is overexpressed in ADPKD patients [13, 14] as well as in mouse models [15] and usually targets the nucleus [13, 14, 16]. Disease progression results in a structural change of the kidney and therefore an oxygen deficiency affecting the cyst-lining cells. Due to the limited oxygen supply, PC1-p30 accumulates in mitochondria and presumably leads to a metabolic shift as well as morphological changes, enabling the cells to remain highly proliferative. This mechanism promotes disease progression of ADPKD. Previous research in the Weimbs Lab has shown that PC1-p30 is expressed and stabilized under hypoxia (Fig. 2.1) and after treatment with cobalt chloride ( $\text{CoCl}_2$ ) (Fig. 2.2), which inhibits the prolyl-hydroxylase domain-containing protein (PHD) [17]. Prolyl hydroxylase domain-containing proteins (PHD) are a family of  $\text{O}_2$ -dependent enzymes that regulate the expression of the hypoxia-inducible factor 1 (HIF1). In the presence of oxygen, PHD hydroxylates proline residues of HIF1- $\alpha$  triggering ubiquitination and proteasomal degradation of the transcription factor [17, 18]. HIF1- $\alpha$  is a subunit of the HIF1 transcription factor, which plays a major role in the adaptive response to hypoxia in mammalian cells [19, 20]. PC1-p30 is expressed if the DOX promotor is induced with DOX (DOX+) but undergoes proteasomal degradation under normoxia (20% oxygen, hypoxia-). It is expressed and stabilized under hypoxic conditions (1% oxygen, hypoxia+) and DOX availability (DOX+).

Under normal oxygen conditions, HIF1- $\alpha$  is expressed constitutively at a low level whereas exposure to hypoxia results in a significant upregulation [21] (Fig. 2.1). Besides hypoxia, cobalt chloride (CoCl<sub>2</sub>) and dimethyloxalylglycine (DMOG) inhibit PHD activity, mimick hypoxia and therefore stabilize HIF1- $\alpha$  [22].

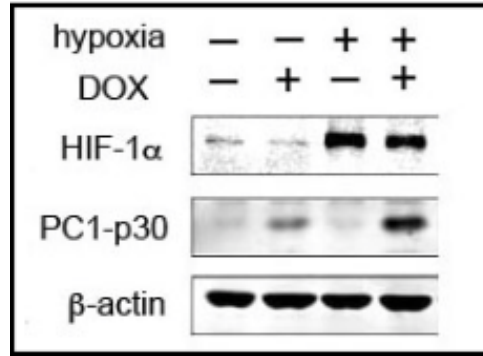


Fig. 2.1: PC1-p30 is stabilized under hypoxic conditions and DOX availability.  $\beta$ -actin functions as a positive control. [preliminary, unpublished data obtained in the Weimbs Lab]

PC1-p30 is expressed if treated with CoCl<sub>2</sub> and DOX is available (DOX+). p30 is similarly expressed after treatment with MG132, an inhibitor reducing the ubiquitination of proteins [23, 24]. HIF-1 $\alpha$  is upregulated after PHD inhibition with CoCl<sub>2</sub> (Fig. 2.2).

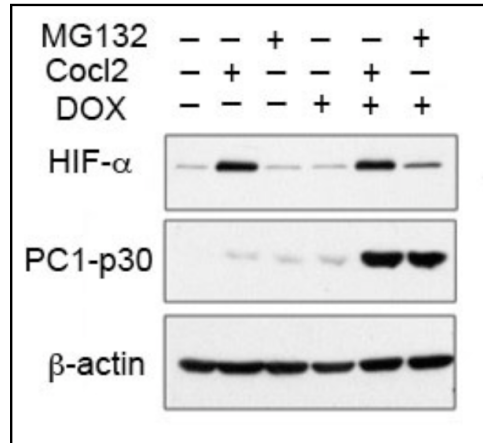


Fig. 2.2: PC1-p30 is stabilized after treatment with the hypoxia-mimicking compound CoCl<sub>2</sub> and DOX availability.  $\beta$ -actin is a loading control. [preliminary, unpublished data obtained in the Weimbs Lab]

Moreover, a smaller fragment of the cytoplasmic tail, PC1-p15 (molecular weight  $\sim$  15 kDa) was found to be overexpressed in ADPKD kidneys [13] and constitutively targets to mitochondria (Fig. 2.3) without inducing hypoxia or inhibiting PHD.

Interestingly, the p16 fragment which is only 12 amino acids longer than p15 shows no mitochondrial targeting, indicating a mitochondria-affecting role of p15.

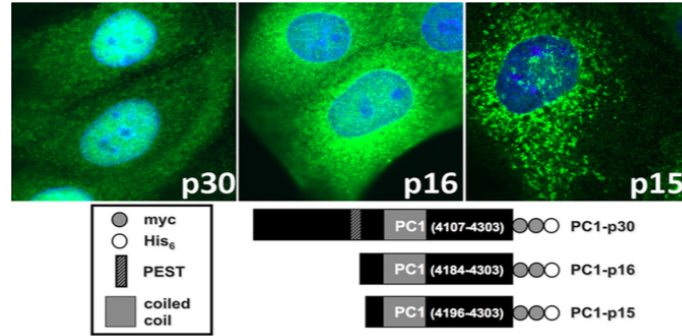


Fig. 2.3: Localization of PC1 C-terminal fragments in normoxia. p15 targets mitochondria constitutively, p30 and p16 localize to the nucleus/cytosol. [preliminary, unpublished data obtained in the Weimbs Lab]

PC1-p30 can activate and interact with the tyrosine kinase protein Src [16], which in turn activates STAT3 signaling [25, 26] (Fig. 2.4). STATs (signal transducers and activators of transcription) are transcription factors which once activated by tyrosine phosphorylation participate in gene regulation [27]. Previous research has shown that the STAT3 pathway is a driving factor for cyst growth in renal epithelial cells [13]. Since targeting the Src/STAT3 activation holds great promise for future therapeutic approaches [7], understanding the regulation of PC1-p30 expression is of major importance.

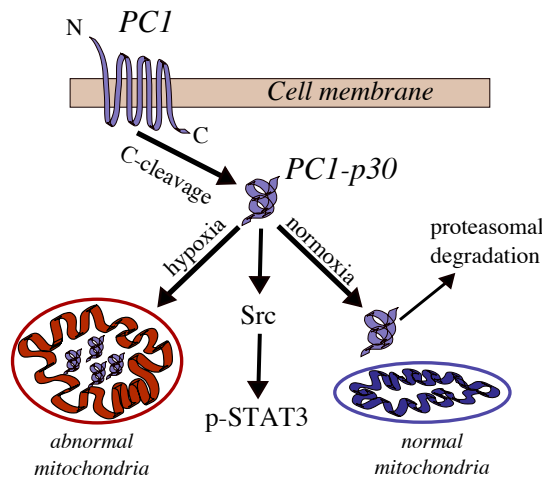


Fig. 2.4: Proposed regulation of mitochondria under hypoxia and normoxia. After being cleaved from PC1 at the C-terminus, PC1-p30 is stabilized under hypoxic conditions but undergoes rapid proteasomal degradation under normoxia. Moreover, PC1-p30 activates Src and therefore also the Src/STAT3 signaling pathway.

PC1-p30 accumulation is caused by defective PC1 signaling. In cyst cells, the accumulation of PC1-p30 may promote a metabolic shift and also changes the shape of mitochondria. It has recently been shown, that defective PC1 signaling caused by knockout of the PKD1 gene which codes for the respective protein results in an altered energy metabolism similar to the Warburg effect exhibited in cancer cells [28]. The Warburg effect is characterized by energy conversion through aerobic glycolysis rather than mitochondrial respiration. Although aerobic glycolysis is a relatively inefficient way of energy generation, most cancer cells predominantly shift to this metabolism even if oxygen is plentiful [29]. Another similarity to cancer cells exhibiting the Warburg effect are the morphological alterations of mitochondria. Previous research in the Weimbs lab has shown, that the expression of PC1-p30 leads to morphological changes that are typical for cells with the Warburg aerobic glycolysis metabolism [30] (Fig. 2.5). In normoxia, PC1-p30 (green) is expressed at a low level and localizes to the nucleus and cytoplasm. Despite the normoxic environment, p30 expression results in morphological alterations of mitochondria resembling the effect in cancer cells exhibiting the Warburg effect (Fig. 2.5, B). Exposing the cells to hypoxia however results strong PC1-p30 expression and mitochondrial targeting (Fig. 2.6, C). When treating the cells with MG132 to prevent proteasomal degradation under normoxia, p30 is strongly expressed but it does not target mitochondria (Fig. 2.6, D).

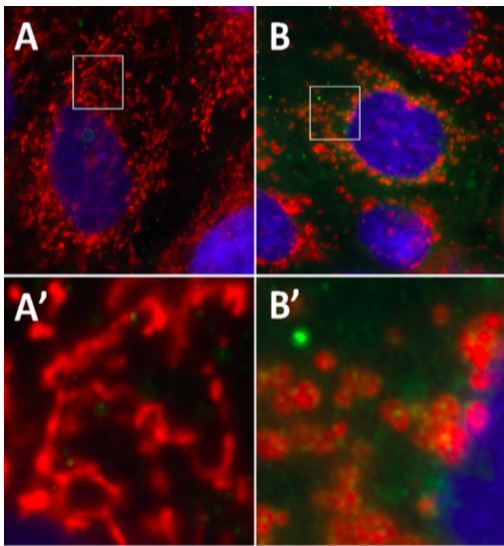


Fig. 2.5: Cells lacking PC1-p30 exhibit normal mitochondria (A). Cells expressing PC1-p30 exhibit globular, fragmented mitochondria (B). (A') and (B') are magnifications of the white squares in (A) and (B). [preliminary, unpublished data obtained in the Weimbs Lab]

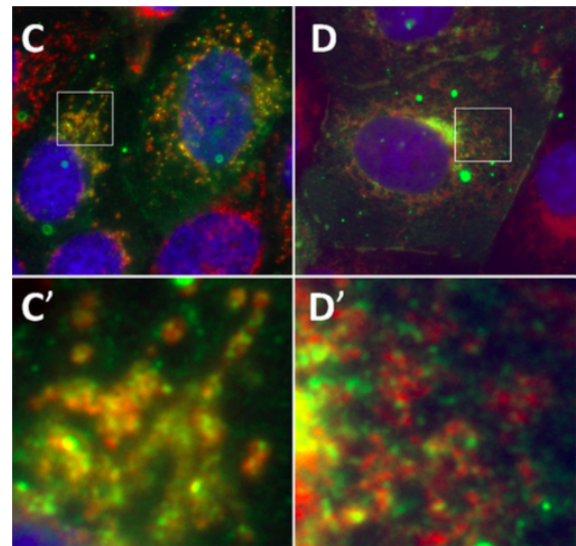


Fig. 2.6: PHD inhibitor with  $\text{CoCl}_2$  results in strong PC1-p30 expression and mitochondrial targeting (C). Proteasome inhibitor with MG132 however results in strong p30 expression but no mitochondrial targeting (D). [preliminary, unpublished data obtained in the Weimbs Lab]

These metabolic and morphological changes enable cyst-lining cells to remain proliferative under hypoxia, promoting disease progression. However, underlying mechanisms remain largely unknown. Besides their function as energy converters, mitochondria also play a key role in inducing apoptosis when facing environmental stress [31]. This stress can develop under hypoxic conditions and normally leads to several apoptosis-inducing mechanisms. In ADPKD however, the changes in mitochondria not only help cells to remain proliferative due to the metabolic shift, but may also promote the adaptation to hypoxia, protecting them against apoptosis-inducing processes. Previous studies have shown, that the adaptation of animals to hypoxia is associated with the suppression of the electron transport chain (ETC) complexes I, II and IV [32]. This results in decreased reactive oxygen species (ROS) production and protection against mitochondrial permeability transition pore (MPTP) opening [32, 33]. ROS, commonly called free radicals, are a natural byproduct of the oxygen metabolism. Among the several reactive oxygen species in cells, the predominant ROS in mitochondria is the superoxide anion ( $O_2^-$ ) [34]. When electrons from reduced substrates are passed from complex I and II to complexes III and IV, protons are pumped across the inner membrane thereby generating a proton gradient which drives ATP synthase. However, approximately 1-3% of the total mitochondrial oxygen is incompletely reduced, resulting in the production of ROS [35]. Primarily, oxygen is converted into superoxide at the level of NADH CoQ reductase (complex I) and CoQ cytochrome C reductase (complex III) of the electron transport chain [36]. At these levels, one single free electron is transferred to molecular oxygen ( $O_2$ ) resulting in the mono-electronic reduction to superoxide  $O_2^-$ . This mechanism is non-enzymatic, however, mitochondrial manganese superoxide dismutase (MnSOD) converts the superoxide anion subsequently to hydrogen peroxide ( $H_2O_2$ ) [37]. The electron leakage and formation of ROS were reported to play an important role in cellular oxidative damage underlying aging and degenerative disease [38, 39]. Exposing cells to hypoxia normally results in an overproduction of ROS, which can lead to fatal cell damage by altering biological macromolecules like DNA, proteins and lipids [40, 41]. MPTP is a pore in the inner mitochondrial membrane, that is closed under normal conditions but opens during certain cellular stress conditions. Once opened, the pore allows passage of any molecule smaller than 1,5 kD. This transition leads to a loss of ionic homeostasis and eventually, cell death [42]. In ADPKD, apoptosis is not induced by these mechanisms, probably due to the alterations of the ETC complexes. In summary, this leads to the hypothesis that the mitochondrial targeting signal of the normally nucleus-targeting PC1-p30 is unmasked under hypoxic conditions, what causes the great accumulation within mitochondria. There, PC1-p30 promotes a metabolic shift similar to the Warburg effect, enabling the cells to remain proliferative irrespective of oxygen availability. Moreover, alterations of ETC complexes lead to the adaptation to hypoxia, protecting the cells against apoptosis-inducing processes. PC1-p15 as part of the PC1 C-terminal tail which constitutively targets mitochondria is proposed to play a similar role in ADPKD regarding impairment of mitochondrial function.

## 3 Experiments

As previous research in the Weimbs lab has shown, PC1-p30 promotes morphological changes in mitochondria, resembling cells with a glycolytic metabolism. Further, it was found that the loss of functional polycystin-1 signaling results in the presumed metabolic shift to increased glycolysis [28]. It was therefore proposed that PC1-p30 expression induces a metabolic shift similar to the Warburg effect observed in cancer cells. PC1-p15 was shown to target constitutively to mitochondria and was therefore proposed to have a similar effect on mitochondrial function. The metabolic alterations may result in hypoxic adaptation, giving the cells the ability to remain proliferative and furthermore protect them against apoptosis.

To this day, there has not emerged a conclusive matter regarding the root cause for the Warburg effect. While Warburg hypothesized that the shift from aerobic respiration to aerobic glycolysis in cancer cells is due to irreversible mitochondrial damage [43, 44], other researchers postulated that the exact reverse was true for the occurrence of the Warburg effect. According to them, the reduced mitochondrial activity stems from the increase in glycolytic flux [45, 46, 47] which was proven to repress mitochondrial respiration by fermentation in yeast cells supplied with high glucose, called the Crabtree effect [48, 49]. In order to elucidate in which way mitochondria are impaired or damaged by PC1-p30 and PC1-p15 in ADPKD, particularly three parameters which provide information about normal or abnormal cellular function were determined. The parameters of choice were the mitochondrial membrane potential (MMP) and reactive oxygen species (ROS) leakage. Further, to test if the PC1-p30 and PC1-p15 expression induces the proposed Warburg-like metabolic shift, data for growth curves was obtained to determine differences in glucose depletion. In parallel, it was measured if differences in the amount of dead, apoptotic and necrotic cells emerge.

### 3.1 Limitations

The strong mitochondrial localization and stabilization of PC1-p30 was observed in cells treated with the hypoxia-mimicking compound  $\text{CoCl}_2$ . However, regarding the testing of mitochondrial function this agent was purposely dismissed as a hypoxia treatment since it has previously been shown that  $\text{CoCl}_2$  causes mitochondrial DNA damage and an increase in ROS generation [50, 51].

It has yet to be dissected which effects exclusively occur due to hypoxia-mimicking and which due to the cytotoxicity of  $\text{CoCl}_2$ . However, the effects of  $\text{CoCl}_2$  would have masked the changes observed in p30 and p15 induced cells. The exposure to real hypoxia was also dismissed due to problems with the implementation. The cells could have been exposed to hypoxia in a hypoxia chamber but treatment and measurements would have taken place in a normoxic environment. The oxygen supply would have restored the normal cell function very quickly making this experiment not feasible. However, it was proposed that the overexpression of PC1-p30 and PC1-p15 was solely sufficient to impair mitochondrial function and the experiments were carried out in normoxia.

### 3.2 Cell Line

Madin-Darby-canine-kidney (MDCK) cells are used to perform the experiments. This cell line is derived from canine epithelial kidney cells, form an epithelial monolayer when grown in culture and hence provide a useful mammalian cell model [52]. The MDCK strain used as non-transfected control cells is a strain isolated from a high passage parental cell line (NBL-2) and is labeled as the clone-II of MDCK cells [53]. The MDCK-II cells were stably transfected with myc-tagged PC1-p30 or PC1-p15 under a doxycycline (DOX)-inducible promoter. Doxycycline is an antibiotic that can be used as a regulating agent in gene expression based on a tetracycline-controlled transcriptional regulation system (Tet-On). Only if DOX is available, the transfected gene for either PC1-p30 or PC1-p15 will be transcribed and the respective protein expressed [54] (Fig. 3.1). Transfected cells were treated with or without DOX to express or suppress gene expression, non-transfected MDCK-II cells were also treated or remained untreated and served as a negative control.

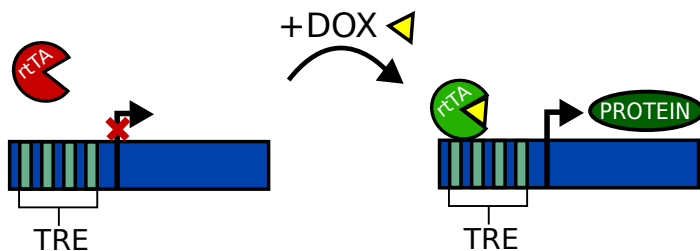


Fig. 3.1: Regulation of gene expression with DOX and Tet-On. Reverse tetracycline-controlled transactivator protein (rtTA) is unbound in the absence of DOX, resulting in an inactive gene. In the presence of DOX, rtTA binds to the TRE (tetracycline-responsive promoter element) and activates gene expression [54].

### 3.3 Mitochondrial Membrane Potential (MMP, $\Delta\Psi_m$ )

The mitochondrial membrane potential (MMP) ( $\Delta\Psi_m$ ) is an electrical potential in form of a proton gradient across the mitochondrial inner membrane, produced by mitochondria to maintain the electron transport chain (ETC). A significant decrease of MMP coincides with the opening of the MPTP, which triggers the apoptotic cascade [55]. Measurements are conducted using the fluorescent dye tetramethylrhodamine, methyl ester (TMRM, Invitrogen™) on live cells. TMRM is a cell-permeable, cationic dye that accumulates in active mitochondria due to their relative negative charge between interior and exterior of the inner mitochondrial membrane. A decrease in MMP will also decrease the accumulation of TMRM and the fluorescent signal dims or disappears [56]. Measurement of MMP therefore gives both information about dysfunction in energy conversion and induction of apoptotic processes. The fluorescent intensity was measured using the BD Accuri C6 flow cytometer (BD Biosciences, USA).

According to Warburg's hypothesis about mitochondrial dysfunction and assuming PC1-p30 and PC1-p15 expression in ADPKD results in a Warburg-like metabolic shift, the membrane potential would decrease in the transfected, induced cells. However, Warburg's hypothesis about mitochondrial dysfunction was later contested since it was shown that the MMP in tumor cells exhibiting the Warburg effect is typically hyperpolarized [57, 58, 59, 60]. The PKD1 knockout in mouse embryonic fibroblasts (MEF cells) however demonstrated no significant difference in MMP compared to wild-type cells [28]. PC1-p30 and PC1-p15 expression was induced by treatment with doxycycline and the results were compared to the MMP of non-induced and non-transfected cells.

### 3.4 Reactive Oxygen Species (ROS)

It is estimated that approximately 90% of the entirety of cellular ROS is generated within mitochondria [61]. There, the superoxide anion, which is the predominant reactive oxygen species in mitochondria is produced as a normal byproduct of oxidative phosphorylation [62, 63]. Since superoxide is generated through the incomplete reduction of oxygen, a mild uncoupling of the electron transport chain means a decrease in leaked protons and therefore lower amounts of oxygen radicals that can be created. The mild uncoupling results in a decrease in MMP, what is consistent with reduced amounts of ROS. A hyperpolarization of the membrane potential leads to an increase in ROS production [61, 64]. Moreover, it was found that superoxide activates the mitochondrial UCP (uncoupling proteins) family [65], indicating a circuit regulation for mitochondrial ROS production.

In normal tissue, superoxide is scavenged to hydrogen peroxide by the mitochondrial targeting enzyme manganese superoxide dismutase (MnSOD) [66, 67]. Several studies have shown that MnSOD is upregulated in cancer cells [68, 69], while others reported the exact opposite [70, 71]. It is therefore still unclear whether and how the expression of MnSOD influences disease progression. The upregulation of MnSOD was shown to sustain the Warburg effect [72] in cancer cells and proposedly in polycystic kidney disease when the C-terminal fragments are expressed. The fluorescent dye MitoSOX Red™ (Invitrogen™) selectively targets mitochondria, where it is oxidized by superoxide but not by other ROS-generating systems. When bound to nucleic acids, the oxidized reagent becomes highly fluorescent [73] which was measured using a flow cytometer (BD Biosciences, USA). Therefore, cells with altered mitochondrial function were distinguished from healthy cells by measuring the mitochondrial superoxide levels.

### 3.5 Proliferation, Cell Survival, Apoptosis and Necrosis

Cells with a glycolytic metabolism highly rely on glucose in order to perform the energy conversion. Therefore, to test the survival and ability to proliferate, transfected MDCK-p30, MDCK-p15 cells and non-transfected control cells were cultured in medium with the usual glucose concentration of 1 g/l and at the same time in medium with a low glucose concentration of 0.1 g/l glucose. The cells were counted using a flow cytometer every 24 to 48 hours to generate a growth curve. Additionally, the cells were stained with Sytox Green Dead Cell Stain (Invitrogen™). The nucleic acid stain is cell-impermeant for cells with an intact cell membrane but can penetrate cells with a compromised membrane and bind to the nucleic acids thereby becoming highly fluorescent. Cell death, primary necrosis and secondary necrosis following apoptosis result in Sytox Green accumulation [74]. To detect if induced cells deplete the glucose in the medium faster and than non-induced cells, the medium was not changed during the growth period. Consistent with this assumption, it was proposed that a faster depletion of nutrients of induced cells leads to a faster decrease in cell count due to the unavailability of nutrients and medium acidification through lactate excretion. The higher amount of dead cells should therefore have also been recognized with the Sytox Green staining.

### 3.6 Data Acquisition: Flow Cytometry

Flow cytometry is a laser-based technology to analyze cells in a suspension. The single cells are transported to the flow chamber in a flow fluid (sheath fluid). Inside the flow chamber, a laser-beam incides onto the cell, which refracts light that is scattered at every angle.

Flow cytometers are equipped with detectors to determine the cell size (forward scatter) and the cell granularity (side scatter). The bigger the cell, the higher is the forward scatter whereas analysis of highly complex cell results in a high side scatter (Fig. 3.2).

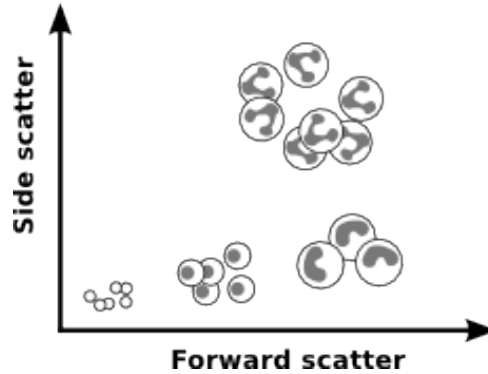


Fig. 3.2: Big cells have a high forward scatter, cells with a high granularity are characterized by a high side scatter. Retrieved from <http://www.bioinformin.net/cytometry/flowplots.php>

Moreover, modern flow cytometers are equipped with lasers of different wavelengths and emission filters to measure fluorescence intensity [75]. Thus, cells stained with fluorescent dyes or bound to fluorescent proteins (e.g. GFP) can be distinguished [76]. Every cell passing through the flow chamber generates a voltage pulse that is displayed as a peak. This peak is characterized by the parameters pulse width, height and area, which is the product of width and height [77]. These parameters are used in data analysis to distinguish cell clumps from single cells. Exclusion of multiplets is crucial in cell analysis as the clumping results in false positive results for fluorescence measurements and is also not representative when using cell count. The generation of duplets and multiplets is the biggest limitation in flow cytometry as the obtained data are only valid and reliable for single cells [78]. If the cell density in the sample is too high, the gating becomes very difficult and the results unreliable. Therefore, cell count was approximated prior to flow analysis using a hemocytometer and the cell suspension was diluted if the cell density exceeded  $1 \times 10^5$  cells/ml. The multiplets were excluded by plotting the side scatter area over the pulse width and an upright rectangle gate was used to distinguish live, single cells as described in Methods. The width of the peak corresponds to the time a cell takes to pass through the laser beam, therefore it is proportional to the cell size. The peak height is the signal intensity detected by the photomultiplier tubes (PMT's) at specific wavelengths. Peak width is independent of the PMT intensity therefore making it the most reliable plot in order to gate single cells [79].

# 4 Methods

## 4.1 Cell Culture

The adherent MDCK cells were cultured in liquid minimum essential medium (MEM, Corning Cellgro) supplied with phenol red, Earle’s salts, 5% fetal bovine serum (FBS), L-glutamine and penicillin-streptomycin on tissue-culture treated culture dishes (Corning Cellgro). The cells were kept in a humidified CO<sub>2</sub> incubator to maintain the pH with a CO<sub>2</sub> concentration of 5% at a temperature of 37° Celsius. To analyze and split the adherent cells, the culture medium was aspirated and the cells were washed with cell culture grade Dulbecco’s Phosphate-Buffered Saline (DPBS, Corning Cellgro) without calcium and magnesium. To dissociate the adherent cells from the culture dish bottom, a mixture of trypsin at a concentration of 0.25% and EDTA was used (Gibco™). Depending on the confluency of the cells, the dishes were incubated for 5-10 minutes in a CO<sub>2</sub> incubator. Trypsin is a digestive protease that cuts adhesion proteins in cell-cell and cell-matrix interactions [80]. However, the serum in the complete medium contains Mg<sup>2+</sup> and Ca<sup>2+</sup> ions which are trypsin inhibitors reducing the dissociation efficiency. EDTA is a chelating agent that sequesters metal ions and therefore increases trypsinization efficiency [81]. Once dissociated, the cells were spun down in a centrifuge, the trypsin/EDTA mix aspirated and the cells were resuspended in complete medium. The obtained single cell suspension was plated at the desired density. The materials and equipment used are listed in Tab. 4.1.

Tab. 4.1: Materials cell culture

organisms	reagents	equipment
MDCK-II cells	MEM	cell culture dishes
MDCK-p30 cells	DPBS	CO <sub>2</sub> incubator
MDCK-p15 cells	FBS	
	L-glutamine	
	penicillin-streptomycin	
	trypsin/EDTA 0.25%	

## 4.2 Mitochondrial Membrane Potential (MMP, $\Delta\Psi_m$ ) assay

Cells were plated and cultured in complete MEM in 24-well plates in either quadruplets or quintuplets and the respective cells were immediately induced with DOX at a concentration of 50  $\mu\text{g}/\text{l}$ . Buffer and medium were warmed to 37°C prior to usage. After 16 to 24 hours of incubation, the cells reached a confluency of 50% and the cells were washed twice with DPBS. Serum and antibiotics can bind stains whereas the pH-indicator phenol red in culture media can produce high autofluorescence and should not be present in the staining medium. Therefore, cells were treated with serum-, antibiotics- and phenol red free MEM with L-glutamine and 20 nM TMRM. TMRM as an extrinsic agent is likely to be rejected by the cell. Therefore, the cells were incubated in the presence of 2  $\mu\text{M}$  of the drug efflux pump P-glycoprotein inhibitor cyclosporin-H [82]. The unstained control cells were treated with the same medium without the TMRM stain. Since TMRM is used at very low concentrations, diminished light conditions were installed during staining. The cells were incubated for 30 minutes at 37°C in the dark in a humidified CO<sub>2</sub> incubator. After 15 minutes of incubation, FCCP was added to the designated wells at a concentration of 4  $\mu\text{M}$ . The plating and treatment pattern is shown in Fig. 4.1. Unstained cells and unstained and stained medium without cells were used as negative controls.

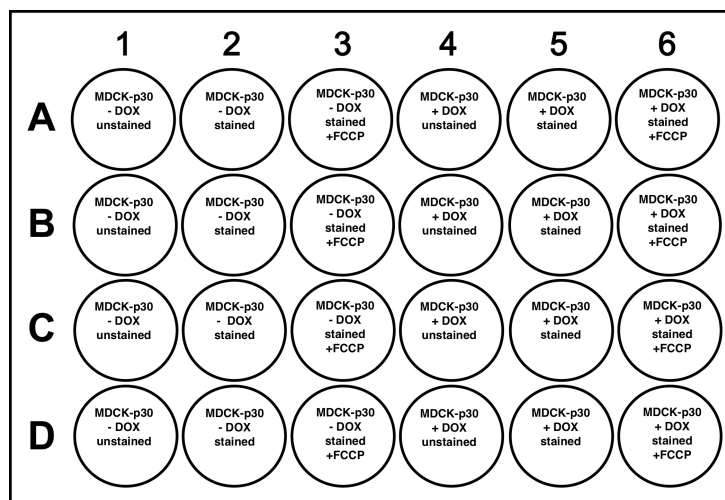


Fig. 4.1: Plating and treatment pattern for the MMP assay exemplarily for MDCK-p30 cells.

FCCP is a mitochondrial electron chain uncoupler [83] used to quantify specifically the mitochondrial membrane potential by eliminating any background fluorescence caused by the dissipated TMRM stain [84]. After the incubation period, the medium was aspirated from all wells and the cells were washed twice with DPBS to increase sensitivity. Thereafter, the adherent cells were dissociated using trypsin/EDTA 0.25% (200  $\mu\text{l}$ ), neutralized with serum-, antibiotics- and phenol red free MEM (300  $\mu\text{l}$ ) and 200  $\mu\text{l}$  of cell suspension of each well were transferred to a 96-well plate with V-bottoms.

The plate was centrifuged at 800 rpm for 2 minutes, the supernatant aspirated and the pellet was resuspended in 150  $\mu$ l serum-, antibiotics- and phenol red free MEM. The samples were analysed on the BD Accuri C6 flow cytometer. Prior to acquisition of each well, the suspension was evenly distributed by pipetting up and down. For each sample, 50  $\mu$ l were acquired and were analysed in fluorescence channel two (FL2) equipped with a 488 nm excitation laser and a 585/40 nm detection filter, matching the fluorescence spectrum of TMRM. Fluorescence intensity was determined by gating on single cells (Fig. 4.2). Multiplets and cell clumps with a higher side scatter area (SSC-A) and higher width were excluded. Particles with a smaller SSC-A and width are debris and cell fragments and were also excluded by gating single cells (Fig. 4.2). SSC-A was plotted over pulse width to obtain a scatter plot for unstained control cells. The single cell population was gated and multiplets and debris are thereby excluded from analysis. The percentage in the gate indicates the proportion of all events represented by the gated events. Event count was plotted over fluorescence intensity to generate a histogram plot for unstained control cells (Fig. 4.3). The same gate as for the single cell population in Fig. 4.2 (R2) was applied to exclusively measure the fluorescence intensity of single cells. The narrow distribution shows the background fluorescence of unstained cells.

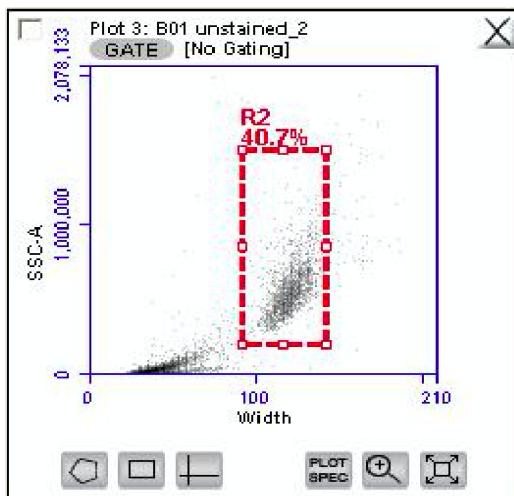


Fig. 4.2: SSC-A over pulse width scatter plot. The single cell population was gated in R2.

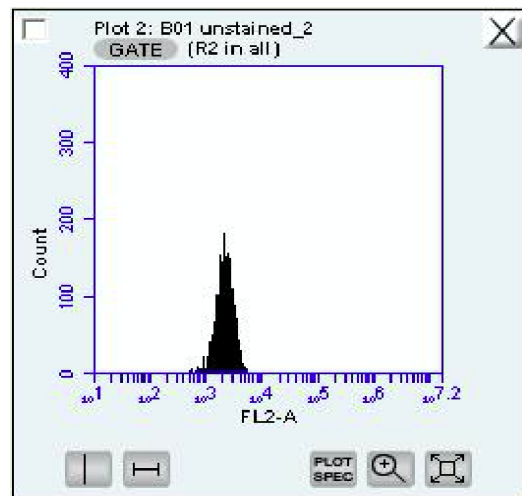


Fig. 4.3: Cell count over fluorescence intensity histogram plot. The peak depicts the background fluorescence of unstained cells. R2 is gated.

For stained samples, the same single cell gate as for unstained cells was applied (Fig. 4.4). The fluorescence intensity of TMRM stained cells clearly shifts to the right (Fig. 4.5). Not all cells take up the dye in the exact same manner resulting in a wider normal distribution compared to unstained cells (Fig. 4.3).

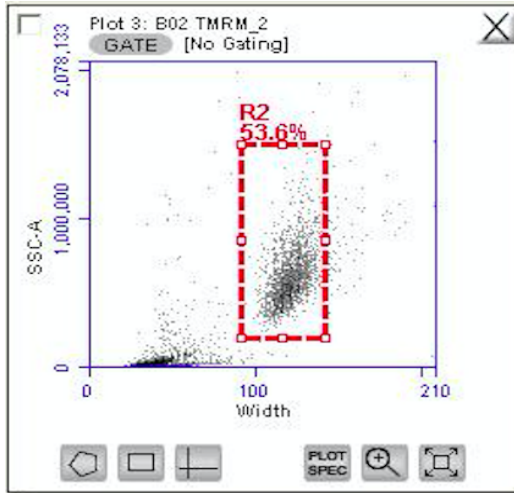


Fig. 4.4: Scatter plot of stained p30 cells. R2 was applied to gate single cells.

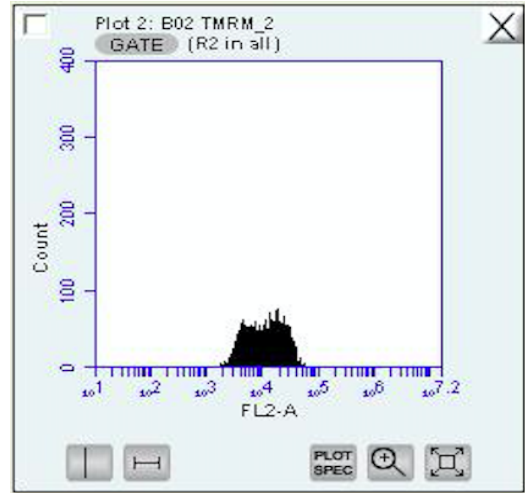


Fig. 4.5: Histogram plot of stained p30 cells. The fluorescent intensity clearly shifts to the right.

The electron transport chain was uncoupled with FCCP to achieve dissipation of TMRM dye due to the low proton gradient. Again, the same single cell gate (R2) was applied (Fig. 4.6). By normalizing the fluorescence intensity of the stained cells to the remaining fluorescent intensity after uncoupling (Fig. 4.7), exclusively the accumulation of TMRM in mitochondria and therefore the relative values for MMP could be determined.

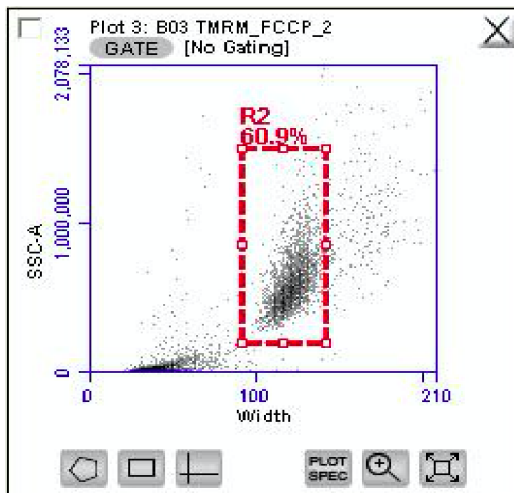


Fig. 4.6: Scatter plot of stained p30 cells treated with FCCP. R2 was applied to gate single cells.

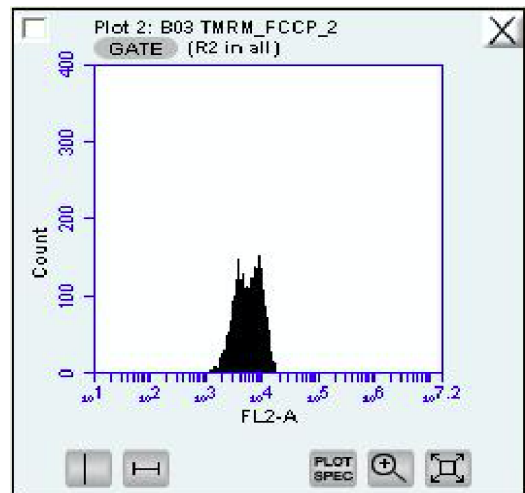


Fig. 4.7: Histogram plot of stained p30 cells treated with FCCP. The fluorescent intensity shifts back to the left.

The quantification of mean fluorescence intensity in all histogram plots was provided by the BD Accuri C6 software and was normalized to the fluorescence intensity of cells treated with FCCP. Measurements were obtained in quadruplets or quintuplets for unstained, stained and uncoupled cells for +/- DOX induced cells respectively. To determine significance of the results comparing induced and non-induced cells, the Student's t-test was used to calculate the p-value. The unpaired t-test was conducted in Microsoft Excel with alpha at 0.05. The materials and equipment used are listed in Tab. 4.2.

Tab. 4.2: Materials MMP assay

organisms	reagents	equipment
MDCK-II cells	doxycycline	24-well plates
MDCK-p30 cells	MEM	96-well plates
MDCK-p15 cells	DPBS	CO <sub>2</sub> incubator
	L-glutamine	BD Accuri C6
	TMRM	microplate centrifuge
	FCCP	
	cyclosporine H	
	trypsin/EDTA 0.25%	

### 4.3 Superoxide detection assay

Cells were plated in 24-well plates in the absence or presence of DOX in complete MEM until reaching a confluency of 50%. Cells were washed twice with DPBS and serum-, antibiotics- and phenol red free MEM with 2  $\mu$ M MitoSox Red was added to the designated wells. Unstained cells as a negative control were incubated in the same conditions without MitoSox Red. In parallel, stained cells were incubated with 50  $\mu$ M antimycin A that served as a positive control. Antimycin A is an inhibitor of the mitochondrial complex III, the primary site of superoxide generation, which was shown to increase the superoxide leakage [85, 86]. The plating and treatment pattern for the superoxide detection assay is shown in Fig. 4.8.

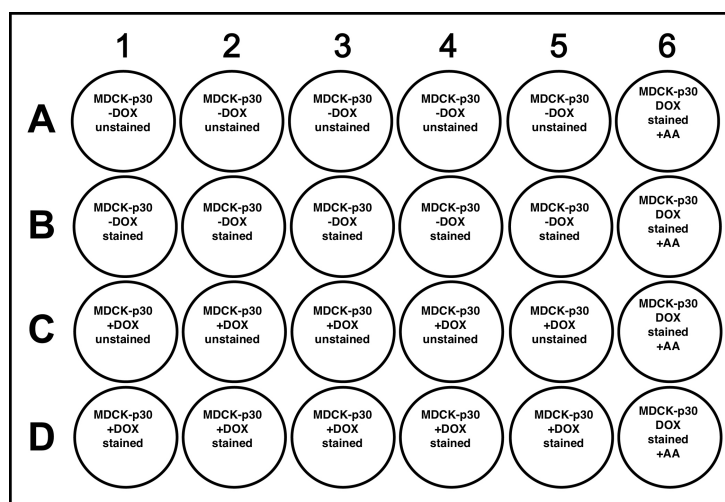


Fig. 4.8: Plating and treatment pattern for superoxide detection with MitoSox Red exemplarily for MDCK-p30 cells.

The procedure from incubation to analysis on the flow cytometer was analogous to the steps in section 4.2. Mean fluorescence intensity of stained cells was measured in FL2 (Fig. 4.10) and was normalized to the autofluorescence of unstained control cells (Fig. 4.9). As described in section 4.2 (Fig. 4.2, 4.4), the single cells were gated and applied to histogram plots determining the mean fluorescence intensity. The peak in Fig. 4.9 depicts the background fluorescence of unstained cells. A single cell gate gated in a SSC-A over pulse width plot was applied (R1). The MitoSox Red stain is oxidized by any existing superoxide and shifts the peak gated in R1 to the right in Fig. 4.10. Measurements were conducted in quintuplets or triplets.

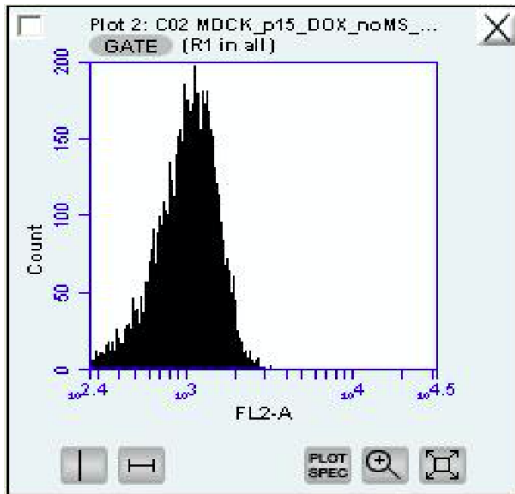


Fig. 4.9: Cell count over fluorescence intensity histogram plot for unstained cells.

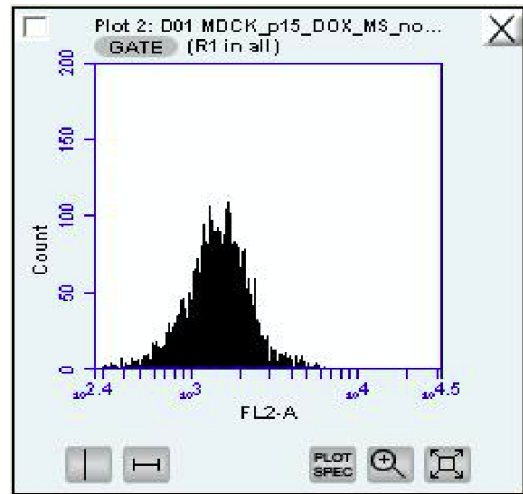


Fig. 4.10: Cell count over fluorescence intensity histogram plot for stained cells.

Treatment with antimycin A shifted the peak to the right (Fig. 4.11) due to the high superoxide leakage. The broad distribution of the peak suggests that the antimycin A induced superoxide leakage varies widely between cells. Statistical significance was calculated using Student's t-test and reported as p-value.

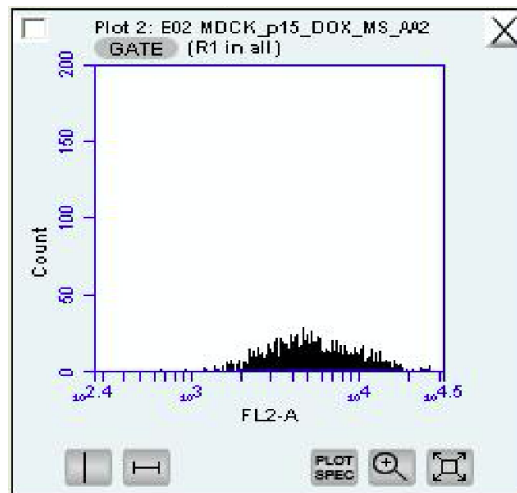


Fig. 4.11: Positive control with antimycin A. Again, the same single cell gate (R1) as for unstained and stained cells was applied.

The materials and equipment used are listed in Tab. 4.3.

Tab. 4.3: Materials superoxide detection assay

organisms	reagents	equipment
MDCK-II cells	doxycycline	24-well plates
MDCK-p30 cells	DPBS	96-well plates
MDCK-p15 cells	MEM	CO <sub>2</sub> incubator
	L-glutamine	BD Accuri C6
	MitoSox Red	microplate centrifuge
	antimycin A	
	trypsin/EDTA 0.25%	

#### 4.4 Growth Curve and Cell Permeabilization detection assay

To adjust the glucose concentration in culture medium, glucose free Dulbecco's modification of MEM (DMEM) was purchased since glucose free MEM was not available. Due to the MDCK cells' adaption to MEM, a sudden switch to a medium with a different composition can have several unwanted effects on the cells such as stress induction or even influence on gene expression [87]. The cells were therefore weaned off MEM over two passages. Cells grown in complete MEM were split and plated on 10 cm dishes with complete 50%/50% (V/V) MEM/DMEM. Once confluent, cells were split and plated on 48-well plates in DMEM supplied with 5% FBS, L-glutamine, penicillin-streptomycin and the respective cells were induced with DOX (50 µg/L). Fig. 4.12 shows the plating and treatment pattern for the assay.

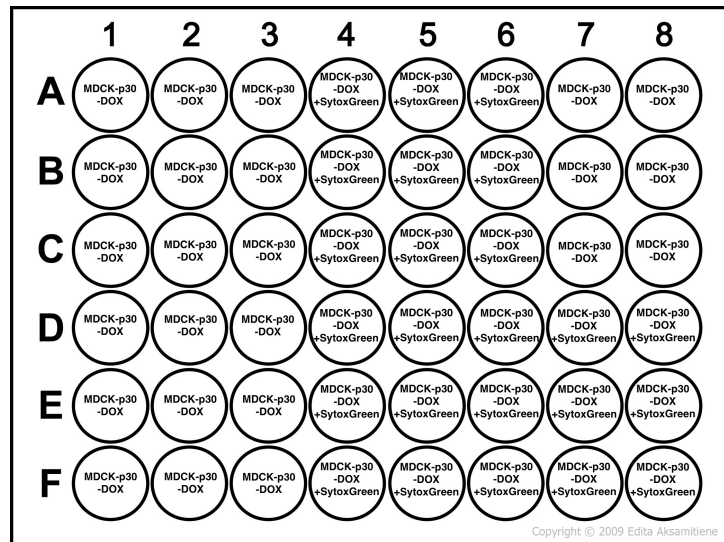


Fig. 4.12: Plating and treatment pattern for the growth curve and cell permeabilization detection exemplarily for MDCK-p30 -DOX cells.

Experiments were carried out culturing cells in medium supplied with a standard glucose concentration of 1 g/l and in parallel the same experiment was conducted by limiting the glucose concentration to 0.1 g/l. DMEM without phenol red was used to avoid high background fluorescence in flow cytometry measurements. Samples were taken from the cell suspension before plating to obtain the cell number at time point zero. Six samples are taken for -/+ DOX respectively. One triplet for -/+ DOX respectively was stained with 30 nM Sytox Green Dead Cell stain and incubated for 25 minutes at room temperature. Heat killed cells were used as a positive staining control, unstained and stained medium without cells was used as a negative control. Samples were then analysed on the BD Accuri C6 flow cytometer in fluorescence channel 1 (FL1), equipped with a 488 nm excitation laser and a 533/30 emission filter. Cell count was obtained by gating on live cells in the SSC-A over pulse width plot. The Accuri software provides cell numbers in events/ $\mu$ l. After applying the single cell gate, the events/ $\mu$ l were multiplied by the dilution volume to obtain the cell count for the entire 48-well plate well. The changes in fluorescence intensity were analyzed in the SSC-A over FL1 plot. Several assay tests prior to the actual data acquisition had shown that, compared to heat killed cells, the sample cells showed very low amounts of actual dead cells but a relatively high amount of necrotic or apoptotic cells. This is due to the dead cells being detached from the monolayer and floating in the medium, therefore mostly being removed during the several washing steps. The stain does not accumulate in apoptotic/necrotic cells as much as in dead cells and the fluorescence intensity of apoptotic/necrotic cells was shown to be only slightly higher than the fluorescence intensity of live cells. The overlap made it therefore difficult to distinguish permeabilized cells from live cells. Based on this exploration, an arbitrary gate was set to a nondimensional fluorescence intensity of  $10^5$  on the FL1 axis and to  $5 \times 10^6$  on the nondimensional SSC-A axis. This gate which compartmentalized the plots in four quadrants was chosen based on the results of several pilot experiments which showed that for all unstained cell samples, more than 99% were gated in the Q1-LL quadrant (Fig. 4.13). Further, the gate separated the healthy cells from stained cells with a relatively high accuracy. The increase in fluorescence intensity, evident as a population shift to the Q1-LR quadrant, corresponds to the proportion of permeabilized cells with regard to live, unstained cells within a single cell population (Fig. 4.14). The proportion is depicted as a relative percentage. Even though the percentage could have been quantified as a cell count, the method was not accurate enough to perform an absolute differentiation of live and permeabilized cells. However, since the main aim was to compare non-induced and induced cells, information about the relative proportion was sufficient for this objective. After every 24 to 48 hours, the medium was aspirated from six wells for -/+ DOX plates respectively, cells were washed twice with DPBS and trypsinized (100  $\mu$ l). Depending on the confluency, between 400 and 1400  $\mu$ l of serum-, antibiotics- and phenol red free DMEM were added to the wells.

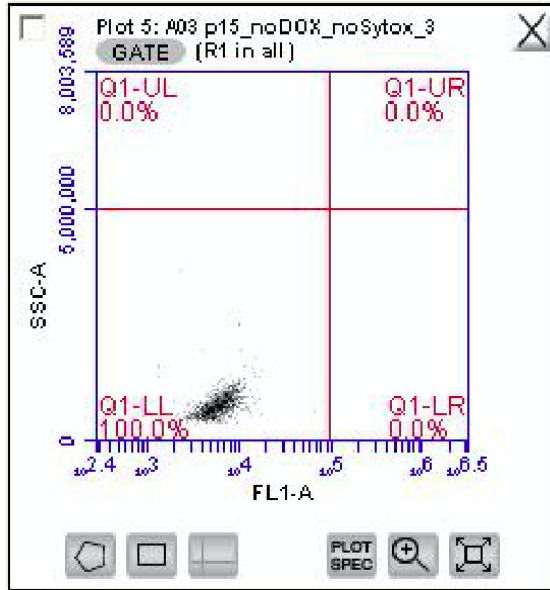


Fig. 4.13: Side scatter area (SSC-A) plotted over the fluorescence intensity in channel 1 (FL1) for unstained cells. The single cell population gate R1 was applied. The entire unstained live cell population was found in Q1-LL.

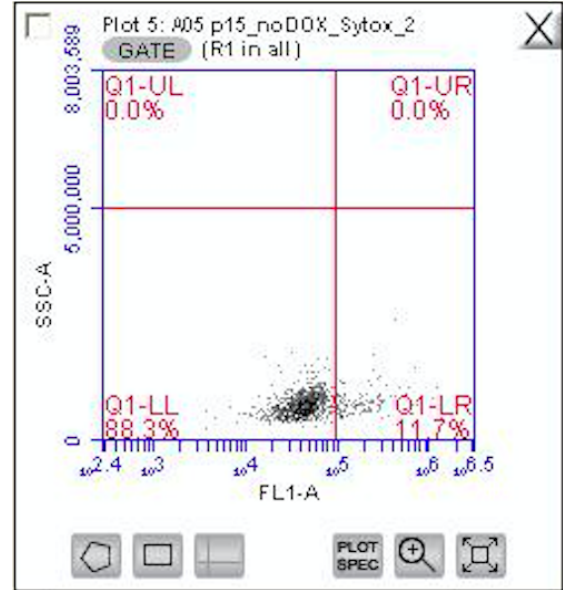


Fig. 4.14: Side scatter area (SSC-A) plotted over the fluorescence intensity in channel 1 (FL1) for stained cells. The entire cell population shifted to the right.

The entire suspension was transferred to 1.5 ml Eppendorf tubes. Cells were stained with 30 nM Sytox Green stain and incubated for 25 minutes at room temperature. Cell count and percentage of permeabilized cells were obtained using the BD Accuri C6 flow cytometer as described above. The experiments was carried out as a batch so the medium was not changed during the growth period. Statistical significance was determined using Student's t-test and reported as p-value. The materials and equipment used are listed in Tab. 4.4.

Tab. 4.4: Materials growth curve and cell permeabilization assay

organisms	reagents	equipment
MDCK-II cells	doxycycline	48-well plates
MDCK-p30 cells	DPBS	CO <sub>2</sub> incubator
MDCK-p15 cells	DMEM	BD Accuri C6
	MEM	Eppendorf tubes
	FBS	microplate centriifuge
	penicillin-streptomycin	
	glucose	
	L-glutamine	
	Sytox Green	
	trypsin/EDTA 0.25%	

# 5 Results

Data are presented as the mean  $\pm$  SD. Student's t-test was used to calculate the p-value as reported in Methods. The significance levels and symbols for the respective p-values are shown in Tab. 5.1. The same levels were used to determine significance in all experiments.

Tab. 5.1: significance levels

symbol	p-value	significance
n.s.	$p \geq 0.5$	not significant
*	$p < 0.5$	significant
**	$p < 0.01$	very significant
***	$p < 0.001$	extremely significant

The standard deviation as a descriptive error bar shows how the data are spread. Even if error bars overlap, it does not provide information about a significant difference between findings, but more about how accurate a measurement was. To determine if two findings are significantly different, the p-value is calculated. A small p-value ( $< 0.05$ ) indicates evidence against the null hypothesis, which is rejected in this case. A p-value larger than 0.05 indicates no evidence against the null hypothesis which can not be rejected [88]. In this experiments, differences between induced and non-induced cells were determined. Based on the proposed effects, the null hypothesis was that there is no difference between induced and non-induced cells expressing PC1-p30 and PC1-p15.

## 5.1 Mitochondrial Membrane Potential

Experiments were conducted three times for MDCK cells stably transfected with PC1-p30 (MDCK-p30) (Fig. 5.1) and non-transfected MDCK cells (MDCK-II) (Fig. 5.3) respectively. Due to temporary reasons, the experiment was carried out twice for MDCK cells transfected with PC1-p15 (MDCK-p15) (Fig. 5.2). The -/+ DOX sets were measured simultaneously, the experiments for cells expressing different protein fragments and non-transfected cells however were done separately.

## 5. Results

Due to widely differing values for TMRM fluorescence in between experiments, the bars of separate experiments were not merged but displayed next to each other. Results for non-induced cells (-DOX) are represented by black bars, white bars show the results for induced cells (+DOX). All data tables are found in the appendix.

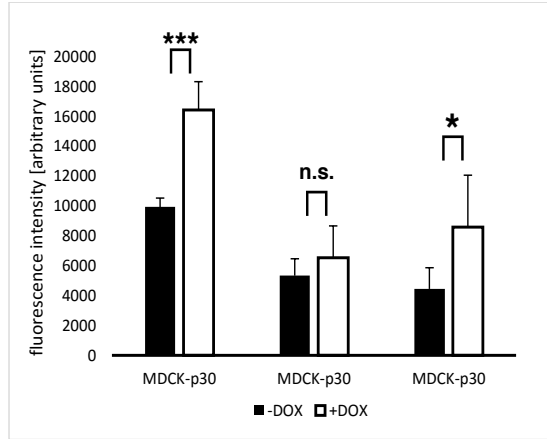


Fig. 5.1: Bars comparing the mean fluorescence intensity determined for non-induced (-DOX) and induced (+DOX) MDCK-p30 cells of three different experiments. Two of the three experiments show a significance difference comparing -/+ DOX cells (Tab. 5.1, data in appendix).

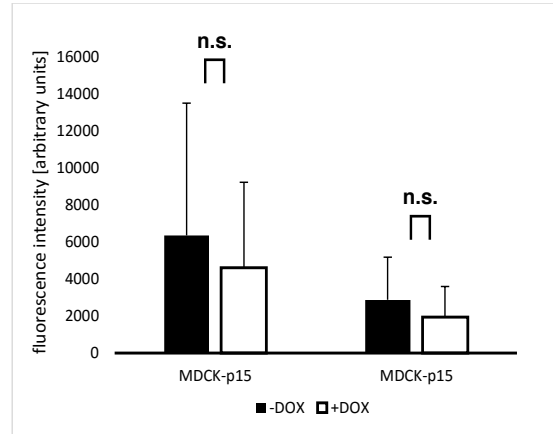


Fig. 5.2: The bars comparing MDCK-p15 -/+ DOX cells of two different experiments show no significant difference in mean fluorescent intensity of the TMRM stain (Tab. 5.2, data in appendix).

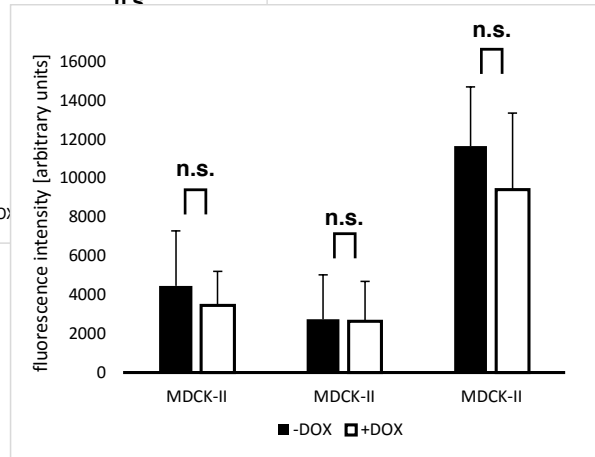


Fig. 5.3: No significant difference between induced and non-induced cells was identified in three different experiments conducted on non-transfected MDCK-II control cells (Tab. 5.6, data in appendix).

## 5.2 Superoxide production

The figures show the results of two separate experiments for MDCK-p30, MDCK-p15 and MDCK-II cells respectively. The fluorescence levels for MitoSox Red differ in between experiments and were not merged therefore. All data tables are found in the appendix.

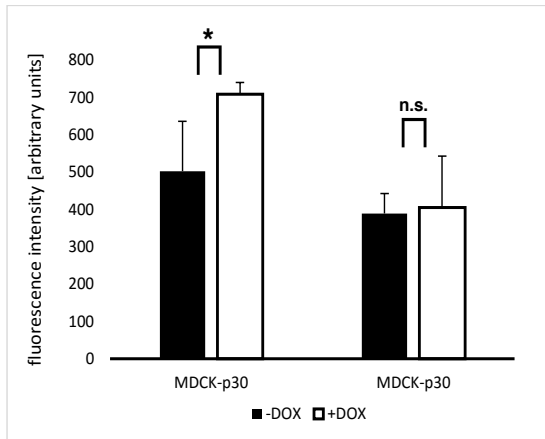


Fig. 5.4: Comparison of mean MitoSox Red fluorescence levels in MDCK-p30 +/- DOX cells for two different experiments. A significant difference in fluorescence levels could be determined for one data set whereas the other experiment did not show significantly different levels in superoxide production (Tab. 5.4, data in appendix).

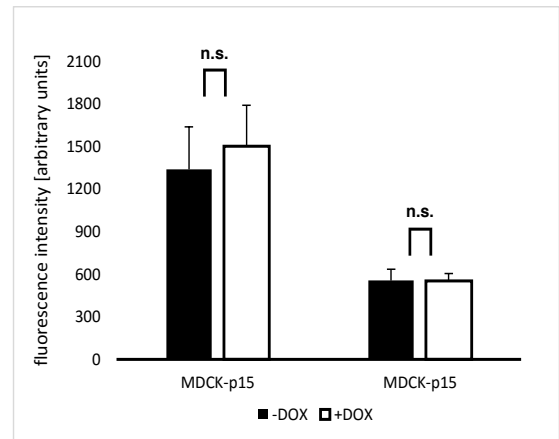


Fig. 5.5: No difference in MitoSox Red mean fluorescence intensity and therefore superoxide levels in MDCK-p15 +/- DOX cells could be determined (Tab. 5.5, data in appendix).

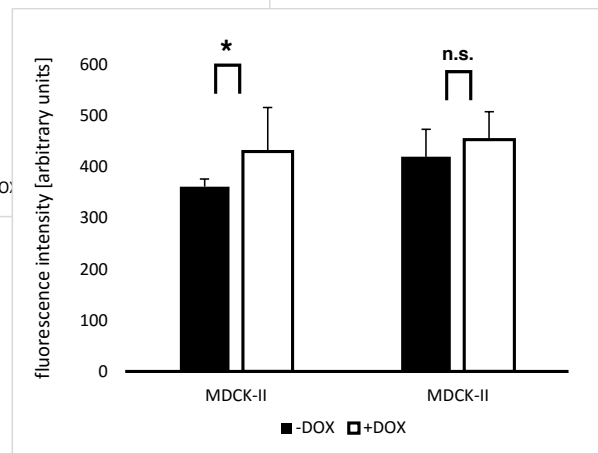


Fig. 5.6: Contrary to the expectations, control MDCK-II cells show a significant difference in superoxide production in one experiment (Tab. 5.6, data in appendix).

### 5.3 Proliferation, Cell Survival, Apoptosis and Necrosis

The term permeabilized cells encompasses dead, apoptotic and necrotic cells as the Sytox Green Dead Cell Stain enters all cells with a compromised membrane [89]. The relative percentage indications correspond to the percentage of permeabilized cells within the single cell population as described in Methods. Black lines represent cells treated with DOX, grey lines correspond to untreated cells. All data are found in the appendix.

#### 5.3.1 MDCK-p30 cells cultured in standard glucose concentration

All cells were cultured in medium with a glucose concentration of 1 g/L. Cells were either untreated (-DOX) or gene expression induced with doxycycline (+DOX, 50 µg/L).

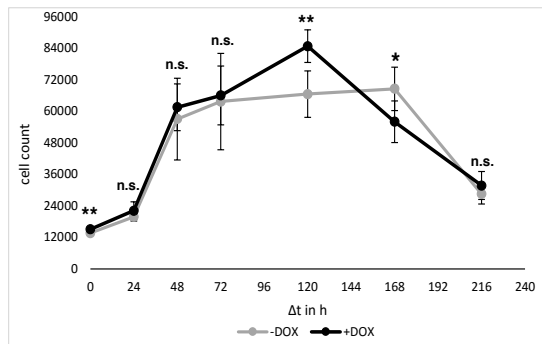


Fig. 5.7: Growth curve for MDCK-p30 cells supplied with 1 g/l glucose. The curve shows significant differences between -/+ DOX induced cells at several time points (Tab. 7, 8, data in appendix).

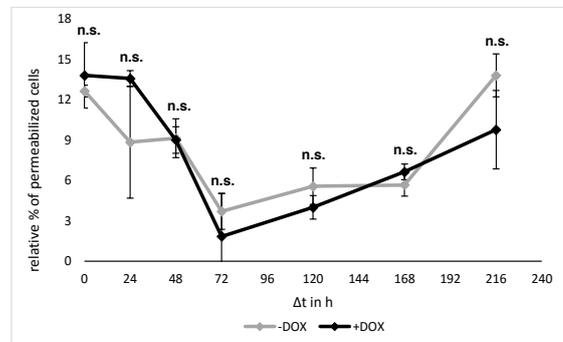


Fig. 5.8: Tracking the amount of permeabilized cells with Sytox Green shows no difference between MDCK-p30 -/+ DOX cells (Tab. 23, data in appendix).

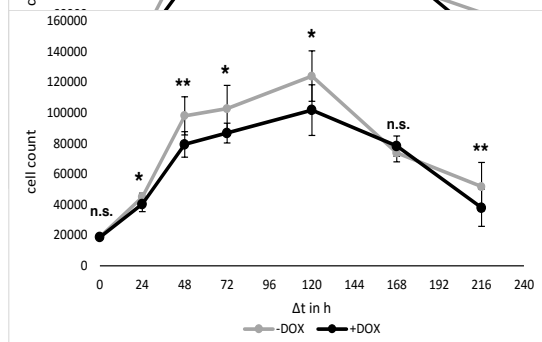


Fig. 5.9: MDCK-II control cells unexpectedly showing differences in proliferation at several time points. Induced cells show a decreased growth rate (Tab. 9, 10, data in appendix).

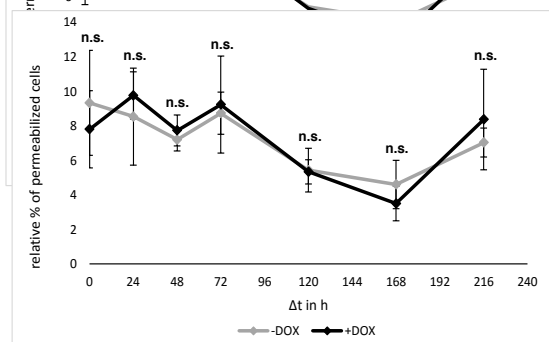


Fig. 5.10: The untreated and DOX treated control cells show no significant difference in apoptotic/necrotic processes (Tab. 24, data in appendix).

### 5.3.2 MDCK-p30 cells cultured in low glucose concentration

The cell culture medium was supplied with 0.1 g/L glucose which is ten times less the concentration used in standard media. DOX was added to the medium to induce cells, -DOX cells lacked doxycycline in the medium to suppress gene expression.

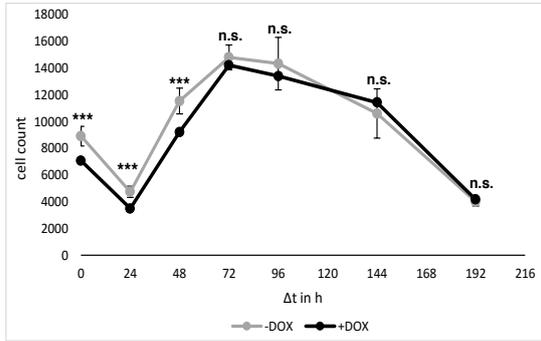


Fig. 5.11: Due to differences in the initial cell counts, the curves for induced and non-induced MDCK-p30 cells show extremely significant differences until the cell number decreases (Tab. 11, 12, data in appendix).

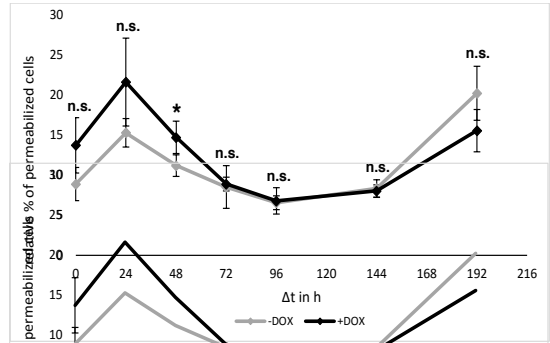


Fig. 5.12: Except for one time point, no significant difference between MDCK-p30 cells +/- DOX could be observed regarding permeabilization of cells (Tab. 25, data in appendix).

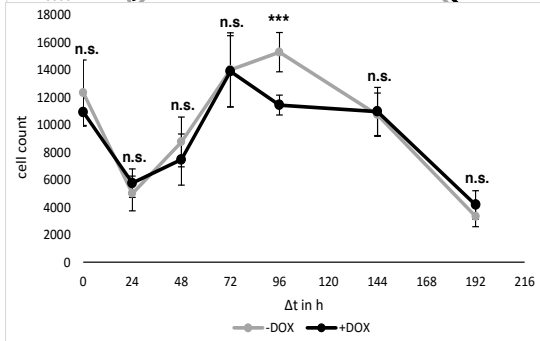


Fig. 5.13: The +/- DOX MDCK-II control cells show a highly significant difference after 102 hours of growth whereas there is no difference at other time points (Tab. 13, 14 data in appendix).

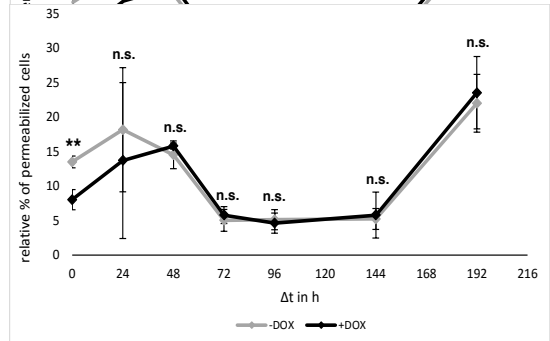


Fig. 5.14: Initially, the amount of permeabilized cells is much higher in untreated MDCK-II control cells. No difference however is evident after the growth onset (Tab. 26, data in appendix).

### 5.3.3 MDCK-p15 cells cultured in standard glucose concentration

The same experiment in section 5.3.1 was conducted for MDCK-p15 cells and MDCK-II control cells cultured in medium with a glucose concentration of 1 g/L.

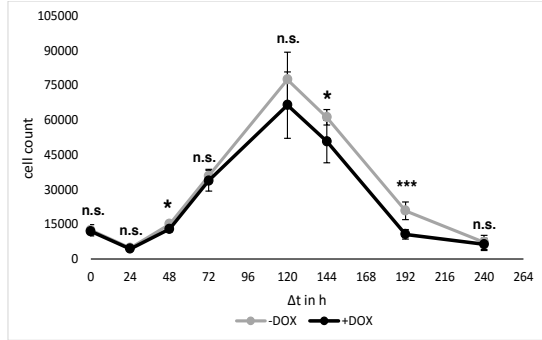


Fig. 5.15: The growth curve for MDCK-p15 cells show differences between cells -/+ DOX at several time points. Both curves decline quickly after reaching the maximal cell count (Tab. 15, 16, data in appendix).

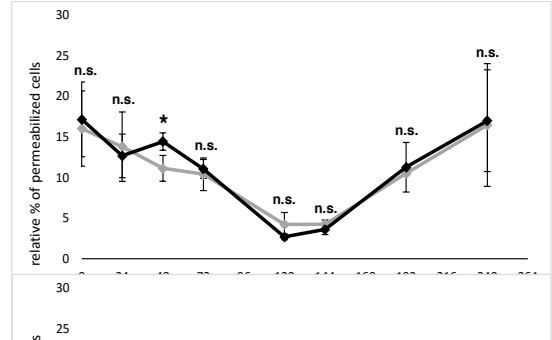


Fig. 5.16: No significant differences in cell permeabilization are evident between MDCK-p15 -/+ DOX cells for most of the growth curve. The significance increase in permeabilized cells in induced cells after 48 hours of growth is consistent with the observation in Fig. 5.15 (Tab. 27, data in appendix).

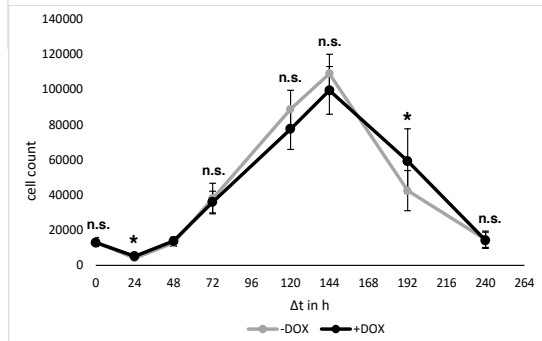


Fig. 5.17: The growth curves for treated and untreated MDCK-II control cells behave very similarly compared to MDCK-p15 cells. Significant differences emerge at two time points (Tab. 17, 18, data in appendix).

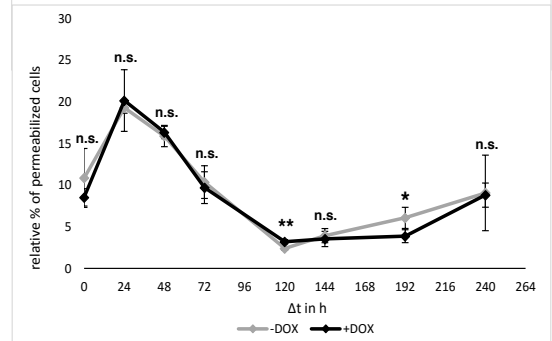


Fig. 5.18: Significant differences emerge at two time points in MDCK-II control cells (Tab. 28, data in appendix).

### 5.3.4 MDCK-p15 cells cultured in low glucose concentration

The same experiment in section 5.3.2 was conducted for MDCK-p15 cells and MDCK-II control cells cultured in medium with a glucose concentration of 0.1 g/L.

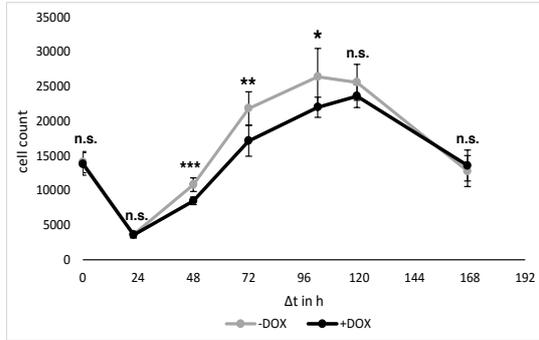


Fig. 5.19: About 24 hours after the growth onset the induced MDCK-p15 cells show a decreased proliferation rate what remains steady until the cell counts start to decline (Tab. 19, 20, data in appendix).

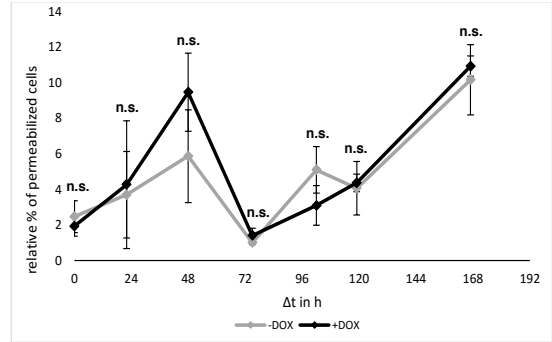


Fig. 5.20: No statistically significant difference regarding the amount of permeabilized cells is evident comparing induced to non-induced MDCK-p15 cells supplied with 0.1 g/L glucose (Tab. 29, data in appendix).

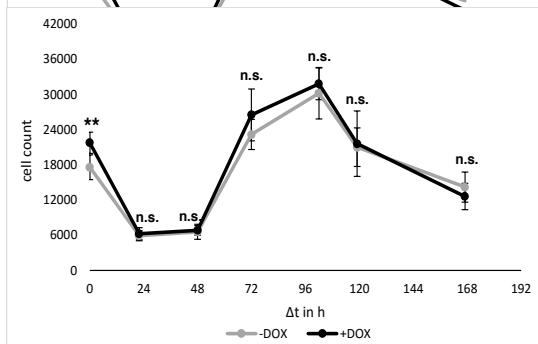


Fig. 5.21: Except for a higher initial cell number of induced MDCK-II control cells, the growth curves overlap with minor deviations (Tab. 21, 22, data in appendix).

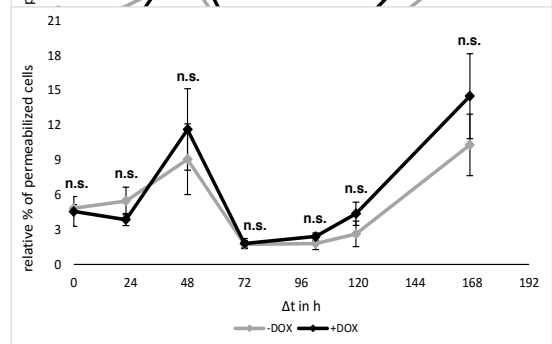


Fig. 5.22: Consistent with the overlapping growth curves of MDCK-II control cells in Fig. 5.21, untreated and DOX-treated cells show no difference in the proportion of dead/necrotic/apoptotic cells (Tab. 30, data in appendix).

## 6 Discussion

Overall, a major pitfall concerning the experiments is the sensitivity and reproducibility of the assays. Even though trends are recognizable, the significance level in several experiments is low or not sufficient to derive a conclusion. Deviations between samples and the resulting large standard deviations might mask any metabolic alteration triggered by the expression of the PC1 C-terminal fragments. An interesting finding that may underlie the inconsistency of the results is that MDCK cells very likely already express the maximal Warburg effect. This assumption is based on the results obtained for the growth curves. Cells cultured in medium with the usual glucose concentration show no or only minor decreases in cell count between time point zero and growth onset (Fig. 5.7, 5.9, 5.15, 5.17). Also, the maximal cell counts are consistently multiple times higher than the initial cell counts, indicating a high proliferation rate in all cells. However, cells expressing the C-terminal fragments as well as control cells proliferate very poorly under limited glucose conditions. After the initial cell counts, a very small proportion of the cell population survives, evident through the sharp decrease after 24 hours (Fig. 5.11, 5.13, 5.19, 5.21). After the growth onset between 24 and 48 hours, the cells do proliferate but poorly. The maximal cell count in all figures is only slightly higher or the same as the initial cell count. This observation suggests that MDCK cells have a high glucose uptake efficiency and metabolize vast amounts of glucose to generate ATP through glycolysis. It has been shown that the predominant energy conversion through aerobic glycolysis is not exclusively found in cancer cells but in most rapidly dividing, permanent cell lines regardless of oxygen availability [92, 93]. Genzel et al. especially examined the bioenergetics in MDCK cells and found that approximately 90% of the metabolized glucose is directly converted into lactate under high glucose concentration and more than 60% go into lactic acid fermentation under low glucose conditions [94]. Even though aerobic glycolysis is less energy efficient in terms of ATP yield compared to aerobic respiration, Vazquez et al. have shown that it is the more favourable metabolic pathway regarding solvent capacity in rapidly proliferating mammalian cells which have a high glucose uptake efficiency [95]. The observation that MDCK cells naturally rely highly on aerobic glycolysis clearly masks a potential influence of p30 and p15 on cellular energy metabolism towards the Warburg-like metabolic shift.

Since the maintenance of the mitochondrial proton gradient is highly dependent on the energy metabolism [96], the exhibition of the Warburg effect in MDCK cells makes it difficult to derive a conclusive interpretation of the obtained results for the mitochondrial membrane potential and the superoxide production in mitochondria.

## 6.1 Mitochondrial Membrane Potential

Obviously, the values for mean fluorescence intensity vary widely in between experiments with the same cells and between experiments on different clones. It is noticeable that the normal distribution of fluorescence intensity in stained cells (Fig. 4.5) is wider compared to the background fluorescence (Fig. 4.3) but also the fluorescent intensity after uncoupling (Fig. 4.7). Since TMRM is a cell-permeant stain that passively diffuses through the membrane, driven by the charged proton gradient in mitochondria, it is very unlikely that the wider distribution of fluorescence intensity in stained cells stems from differences in the stain uptake efficiency [97]. Further, the high standard deviations in mean fluorescence intensity suggest that the stain accumulation varies widely even between single samples of the tested quadruplets. This might mask distinct subpopulations that have altered mitochondrial function. Even though MDCK-p30 and MDCK-p15 are stably transfected, the cell lines go through several passages resulting in genetic variations [90] resulting in differing expression levels of the transfected protein but also metabolic differences due to adaption of some cells resulting in a heterogenous cell population. Especially MDCK-p15 cells demonstrated large standard deviations from the mean. The MDCK-p15 cells used for the MMP experiment went through more passages than the MDCK-p30 and MDCK-II cells which were freshly thawed from low-passage frozen cells prior to analysis. It is therefore very likely that the cells had different p15 expression levels in a heterogenous cell population. This may very likely be the reason for the high variability of fluorescence intensities of the different samples, thereby masking any metabolic change triggered by p15 expression.

A possible explanation for the variations in fluorescence intensities between separate experiments on the same cells is provided by Schieke et al. [91]. This group showed that the progression of the cell cycle through the mitochondrial G1 phase is associated with a significantly higher mitochondrial membrane potential. Especially remarkable is the more than 2-fold increase in MMP for MDCK-II control cells (Fig. 5.3) in experiment 3 compared to the two other experiments. However, results for MDCK-p30 cells not only have smaller standard deviations indicating a more homogenous cell population than in MDCK-p15 cells, but two out of three experiments show a significantly higher mitochondrial membrane potential in cells expressing p30. Experiment 1 shows a very high significance of the result whereas experiment 3 shows significance but at a lower level.

Experiment 2 shows a trend but is not significant, which suggests that several factors such as clonal variation after several passages or the constitutive exhibition of the Warburg effect as described above mask the alterations. This finding of a high mitochondrial membrane potential however is consistent with the observation of hyperpolarized mitochondrial membranes in cancer cells exhibiting the Warburg effect [57, 58, 59], suggesting p30 might actually contribute to the exhibition of the Warburg effect as it was proposed.

## 6.2 Superoxide production

A significant increase of the mitochondrial membrane potential was shown to result in higher ROS leakage [61, 64]. These findings are consistent with the obtained results, showing a significantly increased amount of superoxide in MDCK cells expressing p30 (Fig. 5.4), which were also shown to have elevated levels of mitochondrial membrane potential in two separate experiments (Fig. 5.1). However, while only one out of two experiments on MDCK-p30 cells showed a significant difference in superoxide production, MDCK-II control cells demonstrated a similar result to MDCK-p30 for one experiment at the same significance level. These findings suggest that several factors might have an influence on the ROS leakage, which is not only due to the expression of the PC1 C-terminal fragments. Again, the constitutive exhibition of the Warburg effect which is associated with higher MMP values could mask the metabolic changes caused by the expression of the C-terminal fragments. Again, the differences in fluorescence intensity between experiments on the same cells might stem from the mitochondrial cell cycle progression [91]. Superoxide production is highly dependent of the MMP, which changes during the G1 phase and therefore influences the superoxide leakage. Even though the standard deviations for MDCK-p15 cells are lower, no significant difference between non-induced and induced cells is evident (Fig. 5.5). However, the results for MDCK-p15 cells are consistent with the results for the polarization of the membrane in MDCK-p15 cells which shows no difference between induced and non-induced cells (Fig. 5.2). Nevertheless, it has yet to be tested which role the enzyme MnSOD plays. MnSOD was shown to be upregulated in cancer cells and sustains the Warburg effect [70, 71, 72]. Since superoxide was shown to activate the mitochondrial uncoupling family [65], an upregulation of MnSOD would be reasonable as increased levels of superoxide not only result in cellular damage, but also trigger the apoptotic cascade. The activation of the mitochondrial uncoupling proteins leads to a depolarization of the mitochondrial membrane which coincides with the opening of the mitochondrial permeability transition pore associated with cytochrome c release.

So even if more superoxide is produced as part of the mitochondrial alterations, strongly expressed MnSOD might also scavenge the excess superoxide, prevents the UCP's from being activated and resulting in similar superoxide levels comparing cells expressing p30 and p15 and control cells. This might be a possible protection mechanism employed in polycystic kidney disease due to the expression of the C-terminal fragments.

### 6.3 Proliferation, Cell Survival, Apoptosis and Necrosis

The MDCK-cells already exhibit the Warburg metabolism as described above, what might mask the potential alterations caused by p30 and p15 expression. Apoptosis and necrosis were associated with an increase in mitochondrial ROS production [61]. Cells expressing p30 and p15 did not show consistent elevated levels of superoxide or no increase at all. It is very likely that MnSOD is upregulated as seen in cancer cells exhibiting the Warburg effect and protecting the cells against cell damage. This assumption fits the observations of the Sytox Green staining. Throughout the experiment, no distinct results could be obtained showing higher proportions of dead, apoptotic and necrotic cells when expressing the C-terminal fragments. Neither cells expressing p30 nor induced MDCK-p15 cells show consistent differences in cell count compared to cells with suppressed gene expression under normal glucose conditions. Moreover, control cells also show differences at certain time points. The infrequent significant differences in induced cells and control cells are most likely due to difficulties with the analysis. It is obvious that the infrequent significant differences which are counterintuitive emerge mainly in the stage where cell count declines. Dead cells are fragmented during the preparation process prior to analysis and cause a large amount of debris which also form clumps in the sample. With the progression of the growth curve the gating of single cells becomes difficult and apparently unreliable. Remarkable is the trend observed in induced MDCK-p15 cultured under limited glucose conditions (Fig. 5.19). The cell count shows no difference until 24 hours of growth, after the growth onset however the induced MDCK-p15 cells show a lower proliferation rate. Moreover, even though the standard deviations become larger, the gap between non-induced and induced cells seems to enlarge the more the glucose in the medium is depleted. Compared to the control cells which show no difference except for initial cell count, this observation suggests that p15 expression promotes an even higher dependence on aerobic glycolysis. Another growth curve with consistent differences between induced and non-induced cells was obtained for control cells cultured under standard glucose conditions (Fig. 5.9). It seems like the induced cells show a lower proliferation rate, however a significant difference is already shown after 24 h. Due to treatment or errors in the assay the cell count might just have decreased before the growth onset and fewer cells grew though not having a lower proliferation rate.

Consistent for all experiments is the observation that many cells are not able to attach and grow in culture, resulting in higher amounts of dead, apoptotic and necrotic cells in the beginning. During growth, the amount of permeabilized cells is very low, with the depletion of medium nutrients and extracellular acidification however, the percentage rises again.

## 7 Conclusion

The study by Bonnet et. al [60] showed that cancer cells in solid tumor lines frequently have elevated MMP values and that these levels are associated with aerobic glycolysis and therefore the promotion of the Warburg effect. A model that fits the observations in this project disagrees with Warburg's hypothesized mitochondrial dysfunction in cells exhibiting the effect. It is suggested, that the mitochondrial uncoupling may not primarily be the mechanisms by which cells activate the Warburg effect. Rather are the elevated MMP levels a protection mechanism, as a significant decrease in MMP triggers the apoptotic cascade by opening the mitochondrial permeability transition pore. If superoxide generation per se is increased could not be conclusively be determined in this project and it has to be tested if mitochondrial SOD levels are upregulated. Cell permeabilization coincides with the results for oxidative damage, which was not significantly evident. However, even if ROS production hypothetically was increased due to the higher mitochondrial membrane potential, the consequences would probably be less fatal than the opening of the MPTP.

A trend for a high glucose dependence is apparent in cells expressing p15 under limited glucose conditions. For polycystic kidney disease it is therefore concluded, that p30 and p15 promote a metabolic shift similar to the Warburg effect, characterized by aerobic glycolysis. The expression of the C-terminal fragments does not result in mitochondrial dysfunction, but rather in a hyperpolarization of the mitochondrial membrane that depicts a protection mechanism against opening of the mitochondrial permeability transition pore. Considering that the apoptotic triggering mechanisms are activated during cellular stress conditions including oxygen unavailability, this effect is most likely enhanced in hypoxia. Altogether, this promotes disease progression as cyst lining cells survive rather than being killed in the course of apoptosis. The inconsistent observations however demand for an option to bypass the constitutive Warburg effect in permanent cell lines in order to distinctively extract potential metabolic alterations.

## 8 Future Outlook

Since the main aim was to test if the expression of the polycystin-1 C-terminal fragments promote a Warburg-like metabolic shift characterized by energy conversion mainly through aerobic glycolysis, the experiments demand for a switch to a cell line that generates a higher amount of their energy through aerobic respiration rather than glycolysis. This will increase the sensitivity of the assays and will allow to extract potential metabolic changes as they might not be masked by the natural exhibition of the Warburg effect. Cruz et. al provided data on baby hamster kidney cells, which showed to utilize glucose much more efficiently compared to MDCK cells under low glucose conditions. Under standard glucose conditions, 65% was converted to lactate. Under limiting glucose concentrations at less than 0.1 g/l however, more than 60% was used for respiration [98]. Even though HeLa cells are a permanent cancer cell line, almost 80% percent of their ATP is generated through respiration [99], constituting another potential experimental system. Since both cell lines are permanent, the passaging may have provoked the same glycolysis energy metabolism as in MDCK cells. Respiration will be therefore be measured with a Clark-type oxygen electrode as described in established, published papers [100, 101]. The obtained values will be compared to the literature and if useful, cells will be transfected with p30 and p15 and the above described experiments will be conducted. If the assays are not sensitive enough, a state-of-the-art Seahorse XF Analyzer (Cellular Bioenergetics Core, UCLA) will be used to measure the above named parameters.

Glycolytic cells acidify the medium faster, therefore extracellular acidification will be measured. Further, Rowe et al. demonstrated that the faster medium acidification is visible through a color change of the medium containing the pH-indicator phenol red [28]. Cells will be cultured in a hypoxia chamber and in parallel in normoxia and color changes will be observed and quantified. To determine if the superoxide scavenger MnSOD levels are upregulated under p30 and p15 expression, real time PCR will be performed. For further experiments, the presence of p30 and p15 will be determined with western blotting.

Additionally to flow cytometry, staining experiments with TMRM and MitoSox Red will be conducted using confocal microscopy on live cells as a control but also to check the localization of the used dyes.

To test the effects in hypoxia, the experiments are conducted *in vitro*. Due to the low-oxygen environment, the previously used methods are not feasible. Therefore, mitochondria are isolated from the cells. Following an exposure of 20% and 1% for 24 and 48 hours, the mitochondria are isolated. Subsequently, the respiration rate, activity of complexes I, II, III and IV of the electron transport chain and ROS generation are measured according to established, published protocols [101, 102]. In the future, the stabilization of the C-terminal fragments will be observed *in vivo* using mice exposed to hypoxia or treated with certain pathway inhibitors. Moreover, the effects of p30 and p15 overexpression will be studied in a mouse model with regard to metabolism.

# References

- [1] Wilson, PD. *Polycystic Kidney Disease*.  
N Engl J Med 350, 151-164, 2004.
- [2] Fall, PJ; Prisant, LM. *Polycystic Kidney Disease*.  
The Journal of Clinical Hypertension 7(10), 617–625, 2010.
- [3] Ecker, T; Schrier, RW. *Cardiovascular abnormalities in autosomal-dominant polycystic kidney disease*.  
Nature Reviews Nephrology 5, 221-228, 2009.
- [4] Grantham, JJ. *Autosomal Dominant Polycystic Kidney Disease*.  
N Engl J Med 359, 1477-1485, 2008.
- [5] Grantham, JJ. *Comparison of phenotypes of polycystic kidney disease types 1 and 2*.  
The Lancet 353(9147), 103-107, 1999.
- [6] Bernhardt, WM; Wiesener, MS; Weidemann, A. *Involvement of Hypoxia-Inducible Transcription Factors in Polycystic Kidney Disease*.  
Am J Pathol 170(3), 830–842, 2007.
- [7] Weimbs, T; Talbot, JJ. *STAT3 signaling in polycystic kidney disease*.  
Drug Discovery Today: Disease Mechanisms 10 (3,4), 113-118, 2013.
- [8] Harris, PC; Torres, VE. *Polycystic kidney disease*.  
Annu. Rev. Med. 60, 321-337, 2009.
- [9] Gonzalez-Perrett, S; Kim, K; Ibarra, C; et al. *Polycystin-2, the protein mutated in autosomal dominant polycystic kidney disease (ADPKD), is a Ca<sup>2+</sup>-permeable nonselective cation channel*.  
Proc Natl Acad Sci USA 98, 1182–1187, 2001.
- [10] Koulen, P; Cai, Y; Geng, L; Maeda, Y; Nishimura, S; Witzgall, R; Ehrlich, BE; Somlo, S. *Polycystin-2 is an intracellular calcium release channel*.  
Nat Cell Biol 4, 191–197, 2002.

- [11] Pazour, GJ; Rosenbaum, JL. *Intraflagellar transport and cilia-dependent diseases*. Cell 12(12), 551-555, 2002.
- [12] Chapin, H; Caplan, MJ. *The cell biology of polycystic kidney disease*. J Cell Biol. 191(4), 701–710, 2010.
- [13] Talbot, JJ; Shillingford, JM; Vasanth, S; Doerr, N; Mukherjee, S; Kinter, MT; Watnick, T; Weimbs, T. *Polycystin-1 regulates STAT activity by a dual mechanism*. PNAS 108 (19), 7985-7990, 2011.
- [14] Low, SH; Vasanth, S; Larson, CH; Mukherjee, S; Sharma, N; Kinter, MT; Kane, ME; Obara, T; Weimbs, T. *Polycystin-1, STAT6, and P100 function in a pathway that transduces ciliary mechanosensation and is activated in polycystic kidney disease*. Dev Cell 10 (1), 57-69, 2006.
- [15] Chauvet, V; Tian, X; Husson, H; Grimm, DH; , T; Hiesberger, T; Igarashi, P; Bennett, AM; Ibraghimov-Beskrovnaya, O; Somlo, S; et al. *Mechanical stimuli induce cleavage and nuclear translocation of the polycystin-1 C terminus*. J Clin Invest 114 (10), 1433-1443., 2004.
- [16] Talbot, JJ; Song, X; Wang, X; Rinschen, MM; Doerr, N; LaRiviere, WB; Schermer, B; Pei, YP; Torres, VE; Weimbs, T. *The cleaved cytoplasmic tail of polycystin-1 regulates Src-dependent STAT3 activation*. J Am Soc Nephrol 25 (8), 1737–1748, 2014.
- [17] Matsuura, H; Ichiki, T; Ikeda, J; et al. *Inhibition of Prolyl Hydroxylase Domain-Containing Protein Downregulates Vascular Angiotensin II Type 1 Receptor*. Hypertension 58(3), 354–355, 2011.
- [18] Huang, LE; Gu, J; Schau, M; Bunn, HF. *Regulation of hypoxia-inducible factor 1 $\alpha$  is mediated by an O<sub>2</sub>-dependent degradation domain via the ubiquitin-proteasome pathway*. Proc Natl Acad Sci USA 95(14), 7987–7992, 1998.
- [19] Iyer, NV; Kotch, LE; Agani, F; et al. *Cellular and developmental control of O<sub>2</sub> homeostasis by hypoxia-inducible factor 1 $\alpha$* . Genes Dev. 12(2), 149–162, 1998.
- [20] Wang, GL; Jiang, BH; Rue, EA; Semenza, GL. *Hypoxia-inducible factor 1 is a basic-helix-loop-helix-PAS heterodimer regulated by cellular O<sub>2</sub> tension*. PNAS 92 (12), 5510-5514, 1995.

- [21] Wiener, CM; Booth, G; Semenza, GL. *In Vivo Expression of mRNAs Encoding Hypoxia-Inducible Factor 1*  
Biochemical and Biophysical Research Communications 225(2), 485-488, 1996.
- [22] Siddiq, A; Aminova, LR; Troy, CM. *Selective inhibition of hypoxia-inducible factor prolyl-hydroxylase 1 mediates neuroprotection against normoxic oxidative death via HIF and CREB independent pathways.*  
J Neurosci. 29(27): 8828–8838, 2009.
- [23] Rock, KL; Gramm, C; Rothstein, L; et al. *Inhibitors of the proteasome block the degradation of most cell proteins and the generation of peptides presented on MHC class I molecules.*  
Cell 78(5),761-71,1994.
- [24] Lee, DH; Goldberg, AL. *Proteasome inhibitors: valuable new tools for cell biologists.*  
Cell 8(10), 397-403, 1998.
- [25] Darnell, JE Jr. *STATs and Gene Regulation.*  
Science 277(5332), 1630-1635, 1997.
- [26] Haura, EB. *Roles of activated Src and Stat3 signaling in melanoma tumor cell growth.*  
Oncogene 21, 7001-7010, 2002.
- [27] Turkson, J; Bowman, T; Garcia, R; et al. *Stat3 Activation by Src Induces Specific Gene Regulation and Is Required for Cell Transformation.*  
Mol. Cell. Biol. 18(5), 2545-2552, 1998.
- [28] Rowe, I; Chiaravalli, M; Mannella, V; Ulisse, V; Quilici, G; Pema, M; Song, XW; Xu, H; Mari, S; Qian, F; et al. *Defective Glucose Metabolism in Polycystic Kidney Disease Identifies A Novel Therapeutic Paradigm.*  
Nat Med. 19(4),488–493, 2013.
- [29] Vander Heiden, MG; Cantley, LC; Thompson, CB. *Understanding the Warburg Effect: The Metabolic Requirements of Cell Proliferation.*  
Science 324, 1029-1033, 2009.
- [30] Alirol, E; Martinou, JC. *Mitochondria and cancer: is there a morphological connection?*  
Oncogene 25, 4706–4716, 2006.
- [31] Joza, N; Susin, SA; Daugas, E; Stanford, WL; Cho, SK; Li, CYJ; Sasaki, T; Elia, AJ; Cheng, H-YM; Ravagnan, L; et al. *Essential role of the mitochondrial apoptosis-inducing factor in programmed cell death.*  
Nature 410, 549-554, 2001.

- [32] Ali, SS.; Hsiao, M; Zhao, HW; Dugan, LL; Haddad, GG; Zhou, D. *Hypoxia-Adaptation Involves Mitochondrial Metabolic Depression and Decreased ROS Leakage*. PLoS One, 7(5), e36801, 2012.
- [33] Heather, LC; Cole, MA; Tan, JJ; Ambrose, LJ; Pope, S; Abd-Jamil, AH; Carter, EE; Dodd, MS; Yeoh, KK; Schofield, CJ; Clarke, K. *Metabolic adaptation to chronic hypoxia in cardiac mitochondria*. Basic research in cardiology, 107(3), 1-12, 2012.
- [34] Murphy, MP. *How mitochondria produce reactive oxygen species*. Biochem J 417(1), 1-13, 2009.
- [35] Batandier, C; Fontaine, E; Kériel, C; Leverve, XM. *Determination of mitochondrial reactive oxygen species: methodological aspects*. J Cell Mol Med. 6(2), 175-187, 2002.
- [36] Turrens, JF. *Mitochondrial formation of reactive oxygen species*. J Physiol. 552(2), 335-344. 2003.
- [37] Liu, Y; Fiskum, G; Schubert, D. *Generation of reactive oxygen species by the mitochondrial electron transport chain*. J Neurochem. 80(5), 780-787, 2002.
- [38] Cadenas, E; Davies, KJA. *Mitochondrial free radical generation, oxidative stress, and aging*. Free Radical Biology and Medicine 29(3,4), 222-230, 2000.
- [39] Indo, HP; Yen, HC; Nakanishi, I; et al. *A mitochondrial superoxide theory for oxidative stress diseases and aging*. J Clin Biochem Nutr. 56(1), 1-7, 2015.
- [40] Indo, HP; Davidson, M; Yen, HC; Suenaga, S; Tomita, K; Takeshi, N; Higuchi, M; Koga, Y; Ozawa, T; Majima, HJ. *Evidence of ROS generation by mitochondria in cells with impaired electron transport chain and mitochondrial DNA damage*. Mitochondrion 7, 106-118, 2007.
- [41] Devasagayam, TP; Tilak, JC; Bloor, KK; Sane, KS; Ghaskadbi, SS; Lele, RD. *Free radicals and antioxidants in human health: current status and future prospects*. J Assoc Physicians India 52, 794-804, 2004.
- [42] Halestrap, AP; Clarke, SJ; Javadov, SA. *Mitochondrial permeability transition pore opening during myocardial reperfusion—a target for cardioprotection*. Cardiovascular Research 61, 372-385, 2004.

- [43] Warburg, O. *On the origin of cancer cells.*  
Science 123, 309-314, 1956.
- [44] Chicken or the egg: Warburg effect and mitochondrial dysfunction. *Senyilmaz, D; Teleman, AA.*  
F1000 Prime Rep 7, 41, 2015.
- [45] Weinhouse, S. *The Warburg hypothesis fifty years later.*  
Cancer Res Clin Oncol. 87, 115-126, 1976.
- [46] Weinhouse, S. *On respiratory impairment in cancer cells.*  
Science 124, 267-269, 1956.
- [47] Vander Heiden, MG; Cantley, LC; Thompson, CB. *Understanding the Warburg Effect: The Metabolic Requirements of Cell Proliferation.*  
Science 324, 1029-1033, 2009.
- [48] Crabtree, H. *Observations on the carbohydrate metabolism of tumours.*  
Biochem J. 23, 536-545, 1929.
- [49] Sussman, I; Erecinska, M; Wilson, DF. *Regulation of cellular energy metabolism: the Crabtree effect.*  
Biochim Biophys Acta. 591, 209-223, 1980.
- [50] Wang, G; Hazra, TK; Mitra, S; Lee, HM; Englandera, EW. *Mitochondrial DNA damage and a hypoxic response are induced by CoCl<sub>2</sub> in rat neuronal PC12 cells.*  
Nucleic Acids Res. 28(10), 2135-2140, 2000.
- [51] Zou, W; Yan, M; Xu, W; Huo, H; Sun, L; Zheng, Z; Liu X. *Cobalt chloride induces PC12 cells apoptosis through reactive oxygen species and accompanied by AP-1 activation.*  
J Neurosci Res. 64(6), 646-53, 2001.
- [52] Balcarova-Ständer, J; Pfeiffer, SE; Fuller, SD; Simons, K. *Development of cell surface polarity in the epithelial Madin-Darby canine kidney (MDCK) cell line.*  
EMBO J. 3(11), 2687-2694, 1984.
- [53] Dukes, JD; Whitley, P; Chalmers, AD. *The MDCK variety pack: choosing the right strain*  
BMC Cell Biology, 12:43, 2011.
- [54] Zhu, Z; Zheng, T; Lee, CG; Homer, RJ; Elias, JA. *Tetracycline-controlled transcriptional regulation systems: advances and application in transgenic animal modeling*  
Cell and developmental Biology 13(2), 121-128, 2002.

- [55] Gottlieb, E; Armour, SM; Harris, MH; Thompson, CB. *Mitochondrial membrane potential regulates matrix configuration and cytochrome c release during apoptosis.* Cell Death and Differentiation 10, 709–717, 2003.
- [56] Scaduto, RC Jr; Grotyohann, LW. *Measurement of Mitochondrial Membrane Potential Using Fluorescent Rhodamine Derivatives.* Biophysical Journal 76, 469 –477, 1999.
- [57] Houston, MA; Augenlicht, LH; Heerdt, BG. *Stable differences in Intrinsic Mitochondrial Membrane Potential of Tumor Cell Subpopulations Reflect Phenotypic Heterogeneity.* Int J Cell Bio 2011, 11 pages, 2011.
- [58] Chen, LB. *Mitochondrial membrane potential in living cells.* Annu Rev Cell Biol. 4, 155-181, 1988.
- [59] Davis, S; Weiss, MJ; Wong, JR. *Mitochondrial and Plasma Membrane Potentials Cause Unusual Accumulation and Retention of Rhodamine 123 by Human Breast Adenocarcinoma-derived MDCK-7 cells.* J of Biol Chem 260(25), 13844-13850, 1985.
- [60] Bonnet, S; Archer, SL; Allalunis-Turner, J; et al. *A Mitochondria-K<sup>+</sup> Channel Axis Is Suppressed in Cancer and Its Normalization Promotes Apoptosis and Inhibits Cancer Growth.* Cancer Cell 11(1), 37-51, 2007.
- [61] Balaban, RS; Nemoto, S; Finkel, T. *Mitochondria, Oxidants, and Aging.* Cell, 120, 483–495,2005.
- [62] Batandier, C; Fontaine, E; Kériel, C; Leverve, XM. *Determination of mitochondrial reactive oxygen species: methodological aspects.* J Cell Mol Med. 6(2), 175-187, 2002.
- [63] Kudin, AP; Bimpong-Buta, NY; Vielhaber, S; Elger, CE; Kunz, WS. *Characterization of superoxide-producing sites in isolated brain mitochondria.* J Biol Chem. 279(6), 4127-4135, 2004.
- [64] Brand, MD; Affourtit, C; Esteves, TC; et al. *Mitochondrial superoxide: production, biological effects, and activation of uncoupling proteins.* Free Radical Biology and Medicine 37(6), 755-767, 2004.
- [65] Echtay, KS; Roussel, D; St-Pierre, J; et al. *Superoxide activates mitochondrial uncoupling proteins.* Nature 415, 96-99, 2002.

- [66] Miriyala, S; Spasojevic, I; Tovmasyan, A. *Manganese superoxide dismutase, MnSOD and its mimics*.  
Biochim Biophys Acta 1822(5), 794–814, 2012.
- [67] Christianson, DW. *Structural chemistry and biology of manganese metalloenzymes*.  
Progress in Biophysics and Molecular Biology 67(2-3), 217-243, 1997.
- [68] Borrello, S; De Leo, ME; Galeotti, T. *Defective gene expression of MnSOD in cancer cells*.  
Mol Aspects Med. 14(3), 253-258, 1993.
- [69] Oberley, LW. *Mechanism of the tumor suppressive effect of MnSOD overexpression*.  
Biomedicine & Pharmacotherapy 59(4), 143-148, 2005.
- [70] Izutani, R; Asano, S; Imano, M; et al. *Expression of manganese superoxide dismutase in esophageal and gastric cancers*.  
J Gastroenterol. 33, 816–822, 1998.
- [71] Dhar, SK; Tangpong, J; Chaiswing, L, et al. *Manganese superoxide dismutase is a p53-regulated gene that switches cancers between early and advanced stages*.  
Cancer Res. 71, 6684–6695, 2011.
- [72] Hart, PC; Mao, M; Luelsdorf P. de Abreu, A; et al. *MnSOD upregulation sustains the Warburg effect via mitochondrial ROS and AMPK-dependent signalling in cancer*.  
Nature Communications 6, 6035, 2015.
- [73] Retrieved from: <https://www.thermofisher.com/order/catalog/product/M36008>  
*MitoSOX™ Red Mitochondrial Superoxide Indicator for live-cell imaging*
- [74] Berghe, TV; Vanlangenakker, N; Parthoens, E; et al. *Necroptosis, necrosis and secondary necrosis converge on similar cellular disintegration features*.  
Cell Death and Differentiation 17, 922-930, 2010.
- [75] Adan, A; Günel, A; Kiraz, Y; et al. *Flow cytometry: basic principles and applications*.  
Crit Rev Biotechnol. 37(2), 163-176, 2017.
- [76] Telford, WG; Shcherbakova, DM; Buschke, D; et al. *Multiparametric Flow Cytometry Using Near-Infrared Fluorescent Proteins Engineered from Bacterial Phytochromes*.  
PLoS ONE 10(3), e0122342, 2015.
- [77] Snow, C. *Flow cytometer electronics*.  
Cytometry 57(2), 63-69, 2004.
- [78] Retrieved from: <https://www.bio-rad-antibodies.com/flow-cytometry-doublet-discrimination.html> [22.07.2017] *Doublet Discrimination*

- [79] Shapiro, HM. *Practical Flow Cytometry*. Wiley Online, 2005.
- [80] Rawlings, ND; Barrett, AJ. *Families of serine peptidases*. Methods Enzymol. 244, 19-61, 1994.
- [81] Retrieved from: <http://www.bioind.com/edta-disodium-salt-solution-0-05-in-dpbs/> [07/06/2017] *EDTA Disodium Salt Solution* Biological Industries USA
- [82] Dorababu, M; Nishimura, A; Prabha, T; et al. *Effect of cyclosporine on drug transport and pharmacokinetics of nifedipine*. Biomed Pharmacother. 63(9), 697-702, 2009.
- [83] Retrieved from: <https://meshb.nlm.nih.gov/record/ui?name=FCCP> [11.07.2017] *Carbonyl Cyanide p-Trifluoromethoxyphenylhydrazone* MeSH Descriptor Data 2017
- [84] Rowe, I; Boletta, A. *Mitochondrial Membrane Potential Assay using TMRM*. Bioprotocol 3(23), e987, 2013.
- [85] Quinlan, CL; Gerencser, AA; Treberg, JR; Bran, MD. *The mechanism of Superoxide Production by the Antimycin-inhibited Mitochondrial Q-cycle*. J Biol Chem. 286(36); 31361-31372, 2011.
- [86] Mukhopadhyay, P; Rajesh, M, Yoshihiro, K; et al. *Simple quantitative detection of mitochondrial superoxide production in live cells*. Biochem Biophys Res Commun. 358(1), 203-208, 2007.
- [87] Masters, JR; Stacey, GN. *Changing medium and passaging cell lines*. Nature Protocols 2, 2276-2284, 2007.
- [88] Cumming, G; Fidler, F; Vaux, DL. *Error bars in experimental biology*. Wiley Online, 2005.
- [89] Grootjans, S; Hassannia, B; Delrue, I. *A real-time fluorometric method for the simultaneous detection of cell death type and rate*. Nature Protocols 11, 1444-1454, 2016.
- [90] Pilbrough, W; Munro, TP; Gray, P. *Intraclonal Protein Expression Heterogeneity in Recombinant CHO Cells*. PLoS One, 4(12), e8432, 2009.

- [91] Schieke, SM; McCoy Jr, JP; Finkel, T. *Coordination of mitochondrial bioenergetics with G1 phase cell cycle progression.*  
Cell Cycle 7(12), 1782–1787, 2008.
- [92] Häggström, L. *Cell metabolism, animal.*  
In: Stier R, editor. Encyclopedia of cell technology. New York: Wiley; 392–411, 2000.
- [93] Zu, XL; Guppy, M. *Cancer metabolism: facts, fantasy, and fiction.*  
Biochemical and Biophysical Research Communications 313(3), 459-465, 2004.
- [94] Genzel, Y; Behrendt, I; König, S; et al. *Metabolism of MDCK cells during cell growth and influenza virus production in large-scale microcarrier culture.*  
Vaccine 22(17-18), 2202-2208, 2004.
- [95] Vazquez, A; Liu, J; Oltvai, ZN. *Catabolic efficiency of aerobic glycolysis: The Warburg effect revisited.*  
BMC Systems Biology 4:58, 2010.
- [96] Boland, ML; Chourasia, AH; Macleod, KF. *Mitochondrial Dysfunction in Cancer.*  
Front Oncol. 3(292), 2013.
- [97] Cunningham, CW; Mukhopadhyay, A; Lushington, GH; et al. *Uptake, Distribution and Diffusivity of Reactive Fluorophores in Cells: Implications Toward Target Identification.*  
Mol Pharm. 7(4), 1301–1310, 2010.
- [98] Cruz, HJ; Moreira, JL; Carrondo, MJT. *Metabolic shifts by nutrient manipulation in continuous cultures of BHK cells.*  
Biotechnol. Bioeng. 66 (2), 104-113, 1999.
- [99] Enriquez, SR; Carreno-Fuentes, L; Gallardo-Perez, JC; et al. *Oxidative phosphorylation is impaired by prolonged hypoxia in breast and possibly in cervix carcinoma.*  
The International Journal of Biochemistry and Cell Biology 42, 1744–1751, 2010.
- [100] Andrzejewski, S; Gravel, SP; Pollak, M; et al. *Metformin directly acts on mitochondria to alter cellular bioenergetics*  
Cancer and Metabolism 2:12, 2014.
- [101] Ali, SS.; Hsiao, M; Zhao, HW; et al. *Hypoxia-Adaptation Involves Mitochondrial Metabolic Depression and Decreased ROS Leakage.*  
PLoS One, 7(5), e36801, 2012.
- [102] Heather, LC; Cole, MA; Tan, JJ; et al. *Metabolic adaptation to chronic hypoxia in cardiac mitochondria.*  
Basic research in cardiology, 107(3), 1-12, 2012.

References

---

- [103] Mookerjee, SA; Brand, MD. *Measurement and Analysis of Extracellular Acid Production to Determine Glycolytic Rate.*  
J. Vis. Exp. 106, 2015.

# List of Figures

2.1	stabilization of PC1-p30 in hypoxia . . . . .	3
2.2	stabilization of PC1-p30 after $\text{CoCl}_2$ treatment . . . . .	3
2.3	localization of C-terminal fragments in normoxia . . . . .	4
2.4	regulation of mitochondria in hypoxia compared to normoxia . . . . .	4
2.5	morphological alterations of mitochondria . . . . .	5
2.6	mitochondrial localization of p30 under hypoxia . . . . .	5
3.1	gene regulation with Tet-On . . . . .	8
3.2	side scatter over forward scatter . . . . .	11
4.1	plating pattern for TMRM experiment . . . . .	13
4.2	TMRM: SSC-A over pulse width scatter plot for unstained cells . . . . .	14
4.3	TMRM: cell count over fluorescence intensity histogram plot for unstained . . . . .	14
4.4	TMRM: SSC-A over pulse width scatter plot for stained cells . . . . .	15
4.5	TMRM: cell count over fluorescence intensity histogram plot for stained cells . . . . .	15
4.6	TMRM: SSC-A over pulse width scatter plot for stained cells treated with FCCP . . . . .	15
4.7	TMRM: cell count over fluorescence intensity histogram plot for stained cells treated with FCCP . . . . .	15
4.8	plating pattern for MitoSox experiment . . . . .	17
4.9	MitoSox: cell count over fluorescence intensity histogram plot for unstained cells . . . . .	18
4.10	MitoSox: cell count over fluorescence intensity histogram plot for stained cells . . . . .	18
4.11	MitoSox: cell count over fluorescence intensity histogram plot for stained cells treated with antimycin A . . . . .	18
4.12	plating pattern for growth curve and cell permeabilization detection . . . . .	19
4.13	Sytox: SSC-A over fluorescence intensity plot for unstained cells . . . . .	21
4.14	Sytox: SSC-A over fluorescence intensity plot for stained cells . . . . .	21
5.1	TMRM fluorescence levels for three different experiments in MDCK-p30 cells . . . . .	23
5.2	TMRM fluorescence levels for two different experiments in MDCK-p15 cells . . . . .	23
5.3	TMRM fluorescence levels for three different experiments in MDCK-II cells . . . . .	23
5.4	MitoSOX Red fluorescence levels for two different experiments in MDCK-p30 cells . . . . .	24
5.5	MitoSOX Red fluorescence levels for two different experiments in MDCK-p15 cells . . . . .	24
5.6	MitoSOX Red fluorescence levels for two different experiments in MDCK-II cells . . . . .	24
5.7	growth curve for MDCK-p30 +/- DOX cells cultured in medium with a standard glucose concentration . . . . .	25

5.8	proportion of dead, apoptotic and necrotic cells in MDCK-p30 -/+ DOX cells in standard glucose . . . . .	25
5.9	growth curve for MDCK-II -/+ DOX control cells for MDCK-30 cells cultured in medium with a standard glucose concentration . . . . .	25
5.10	proportion of dead, apoptotic and necrotic cells in MDCK-II -/+ DOX control cells for MDCK-p30 cells in standard glucose . . . . .	25
5.11	growth curve for MDCK-p30 -/+ DOX cells cultured in medium with a low glucose concentration . . . . .	26
5.12	proportion of dead, apoptotic and necrotic cells in MDCK-p30 -/+ DOX cells in low glucose . . . . .	26
5.13	growth curve for MDCK-II -/+ DOX control cells for MDCK-p30 cells cultured in medium with a low glucose concentration . . . . .	26
5.14	proportion of dead, apoptotic and necrotic cells in MDCK-II -/+ DOX control cells for MDCK-p30 cells in low glucose . . . . .	26
5.15	growth curve for MDCK-p15 -/+ DOX cells cultured in medium with a standard glucose concentration . . . . .	27
5.16	proportion of dead, apoptotic and necrotic cells in MDCK-p15 -/+ DOX cells in standard glucose . . . . .	27
5.17	growth curve for MDCK-II -/+ DOX control cells for MDCK-p15 cells cultured in medium with a standard glucose concentration . . . . .	27
5.18	proportion of dead, apoptotic and necrotic cells in MDCK-II -/+ DOX control cells for MDCK-p15 cells in standard glucose . . . . .	27
5.19	growth curve for MDCK-p15 -/+ DOX cells cultured in medium with a low glucose concentration . . . . .	28
5.20	proportion of dead, apoptotic and necrotic cells in MDCK-p15 -/+ DOX cells in low glucose . . . . .	28
5.21	growth curve for MDCK-II -/+ DOX control cells for MDCK-p15 cells cultured in medium with a low glucose concentration . . . . .	28
5.22	proportion of dead, apoptotic and necrotic cells in MDCK-II -/+ DOX control cells for MDCK-p15 cells in low glucose . . . . .	28

# List of Tables

4.1	Materials cell culture . . . . .	12
4.2	Materials MMP assay . . . . .	16
4.3	Materials superoxide detection assay . . . . .	19
4.4	Materials growth curve and cell permeabilization assay . . . . .	21
5.1	significance levels . . . . .	22
1	data for MMP assays on MDCK-p30 cells . . . . .	xviii
2	data for MMP assays on MDCK-p15 cells . . . . .	xix
3	data for MMP assays on MDCK-II control cells . . . . .	xx
4	data for superoxide detection assays on MDCK-p30 cells . . . . .	xxi
5	data for superoxide detection assays on MDCK-p15 cells . . . . .	xxii
6	data for superoxide detection assays on MDCK-II control cells . . . . .	xxiii
7	data for growth curve assay on MDCK-p30 cells in standard glucose . . . . .	xxiv
8	data for growth curve assay on MDCK-p30 cells in standard glucose extension . . .	xxv
9	data for growth curve assay on MDCK-II control cells for MDCK-p30 cells in standard glucose . . . . .	xxvi
10	data for growth curve assay on MDCK-II control cells for MDCK-p30 cells in standard glucose extension . . . . .	xxvii
11	data for growth curve assay on MDCK-p30 cells in low glucose . . . . .	xxviii
12	data for growth curve assay on MDCK-p30 cells in low glucose extension . . . . .	xxix
13	data for growth curve assay on MDCK-II control cells for MDCK-p30 cells in low glucose . . . . .	xxx
14	data for growth curve assay on MDCK-II control cells for MDCK-p30 cells in low glucose extension . . . . .	xxxi
15	data for growth curve assay on MDCK-p15 cells in standard glucose . . . . .	xxxii
16	data for growth curve assay on MDCK-p15 cells in standard glucose extension . .	xxxiii
17	data for growth curve assay on MDCK-II control cells for MDCK-p15 cells in standard glucose . . . . .	xxxiv
18	data for growth curve assay on MDCK-II control cells for MDCK-p15 cells in standard glucose extension . . . . .	xxxv
19	data for growth curve assay on MDCK-p15 cells in low glucose . . . . .	xxxvi
20	data for growth curve assay on MDCK-p15 cells in low glucose extension . . . . .	xxxvii
21	data for growth curve assay on MDCK-II control cells for MDCK-p15 cells in low glucose . . . . .	xxxviii

22	data for growth curve assay on MDCK-II control cells for MDCK-p15 cells in low glucose extension . . . . .	xxxix
23	data for cell permeabilization assay on MDCK-p30 cells in standard glucose . . . . .	xl
24	data for cell permeabilization assay on MDCK-II control cells for MDCK-p30 cells in standard glucose . . . . .	xli
25	data for cell permeabilization assay on MDCK-p30 cells in low glucose . . . . .	xlii
26	data for cell permeabilization assay on MDCK-II control cells for MDCK-p30 cells in low glucose . . . . .	xliii
27	data for cell permeabilization assay on MDCK-p15 cells in standard glucose . . . . .	xliv
28	data for cell permeabilization assay on MDCK-II control cells for MDCK-p15 cells in standard glucose . . . . .	xlv
29	data for cell permeabilization assay on MDCK-p15 cells in low glucose . . . . .	xlvi
30	data for cell permeabilization assay on MDCK-II control cells for MDCK-p15 cells in low glucose . . . . .	xlvii

# List of Abbreviations

abbreviation	description
PC1	polycystin-1
PC2	polycystin-2
STAT	signal transducer and activator of transcription
ROS	reactive oxygen species
MDCK cells	Madin Darby canine kidney cells
DOX	doxycycline
MnSOD	mitochondrial manganese superoxide dismutase
ETC	electron transport chain
MPTP	mitochondrial permeabilization transition pore
ADPKD	autosomal dominant polycystic kidney disease
MMP	mitochondrial membrane potential
$\Delta\Psi_m$	mitochondrial membrane potential
TMRM	tetramethylrhodamine, methyl ester
UCP	uncoupling protein
FCCP	Carbonyl cyanide-p-trifluoromethoxyphenylhydrazone
MEM	minimal essential medium
FBS	fetal bovine serum
p30	C-terminal protein fragment PC1-p30
p15	C-terminal protein fragment PC1-p15

# Appendix

- data tables mitochondrial membrane potential (MMP assays)
- data tables superoxide detection assays
- data tables growth curve
- data tables cell permeabilization (Sytox Green staining)

Annotation: All data for fluorescent staining in the following tables obtained on the BD Accuri C6 flow cytometer have arbitrary units unless otherwise specified.

## mitochondrial membrane potential

Tab. 1: data for MMP assays on MDCK-p30 cells

	p30_noDOX unstained	p30_noDOX TMRM	p30_noDOX TMRM_FCCP	p30_DOX unstained	p30_DOX TMRM	p30_DOX TMRM_FCCP	p-value
EXP1							
26-May	1324.79	15458.84	5217.65	1370.80	23165.26	6474.23	
	1264.15	15971.10	5735.28	1677.16	24002.39	5849.16	
	2100.34	15500.73	5304.84	1617.30	23254.20	6244.47	
	1491.77	15244.43	5623.10	1852.84	21774.38	6214.87	
	1477.27	14920.65	5543.99	1869.67	20270.22	5440.83	
mean	1531.66	15419.15	5484.97	1677.55	22493.29	6044.71	
STD		384.68	217.44		1480.44	405.05	
absolute mean		<b>9934.18</b>			<b>16448.58</b>		
absolute STD		<b>602.12</b>			<b>1885.49</b>		
							<b>&lt;0.001</b>

	p30_noDOX unstained	p30_noDOX TMRM	p30_noDOX TMRM_FCCP	p30_DOX unstained	p30_DOX TMRM	p30_DOX TMRM_FCCP	p-value
EXP2							
31-May	3041.78	12933.86	7441.26	3142.13	13959.89	7236.64	
	3114.29	14234.94	7752.66	3050.64	15115.78	7625.99	
	2922.64	12027.69	7593.56	3120.17	13427.57	7325.71	
	3058.67	12339.08	7406.80	2994.10	11743.95	5949.69	
mean	3034.35	12883.89	7548.57	3076.76	13561.80	7034.51	
STD		976.00	158.42		1401.89	742.14	
absolute mean		<b>5335.32</b>			<b>6527.29</b>		
absolute STD		<b>1134.42</b>			<b>2144.04</b>		
							<b>0.11</b>

	p30_noDOX_unstained	p30_noDOX_TMRM	p30_noDOX_TMRM_FCCP	p30_DOX_unstained	p30_DOX_TMRM	p30_DOX_TMRM_FCCP	p-value
EXP3							
2-Jun	2242.57	10240.31	5076.28	2256.00	18643.56	6303.80	
	2182.03	9951.75	4866.53	2228.29	14686.20	6418.12	
	2194.36	9457.67	4732.54	2285.91	13693.78	6072.85	
	2351.15	7488.51	4666.46	2287.09	11473.30	5346.21	
mean	2242.53	9284.56	4835.45	2264.32	14624.21	6035.25	
STD		1240.21	180.84		2997.39	481.28	
absolute		<b>4449.11</b>			<b>8588.97</b>		
absolute STD		<b>1421.05</b>			<b>3478.67</b>		
							<b>0.02</b>

Tab. 2: data for MMP assays on MDCK-p15 cells

	p15_noDOX unstained	p15_noDOX TMRM	p15_noDOX TMRM_FCCP	p15_DOX unstained	p15_DOX_TMRM	p15_DOX TMRM_FCCP	p-value
EXP1							
15-Jul	1758.64	20855.79	7137.05	1874.81	16885.99	6982.6	
	1913.23	14471.00	6497.99	1805.00	13323.73	7179.32	
	2076.44	9474.29	5167.09	1955.47	9870.12	6269.19	
	2208.22	9002.49	5684.28	1987.36	6941.44	6161.27	
	2129.36	6098.24	3612.17	2558.98	8445.01	5736.43	
mean	2017.18	11980.36	5619.72	2036.324	11093.26	6465.76	
STD		5803.53	1352.12		4008.67	599.91	
<b>absolute mean</b>		<b>6360.65</b>			<b>4627.50</b>		
<b>absolute STD</b>		<b>7155.66</b>			<b>4608.58</b>		
							<b>0.30</b>

	p15_noDOX unstained	p15_noDOX TMRM	p15_noDOX TMRM_FCCP	p15_DOX unstained	p15_DOX TMRM	p15_DOX TMRM_FCCP	p-value
EXP2							
16-Jul	1676.14	9080.01	3928.72	1808.21	7528.29	4004.75	
	1658.17	7217.74	3882.58	1667.90	5773.78	3934.88	
	1711.71	5567.88	2665.38	1820.19	5103.31	3199.21	
	1751.71	5133.29	3584.75	1680.94	4420.82	3285.96	
	1786.81	4779.13	3304.48	1962.31	4535.74	3263.51	
mean	1716.91	6355.61	3473.18	1787.91	5472.39	3537.66	
STD		1786.44	516.86		1268.55	396.55	
<b>absolute mean</b>		<b>2882.43</b>			<b>1934.73</b>		
<b>absolute STD</b>		<b>2303.30</b>			<b>1665.10</b>		
							<b>0.18</b>

Tab. 3: data for MMP assays on MDCK-II control cells

	11_noDOX unstained	11_noDOX TMRM	11_noDOX TMRM_FCCP	11_DOX unstained	11_DOX TMRM	11_DOX TMRM_FCCP	p-value
EXP1							
1-Jun	3143.43	25258.19	10684.86	2631.69	15916.34	8315.15	
	3093.39	22778.77	11168.38	2720.77	13701.25	8686.87	
	3407.54	20636.60	11185.65	2570.25	19474.56	8000.57	
	3303.21	20429.22	9482.69	2655.74	20485.57	6877.17	
mean	3236.89	22275.70	10630.40	2644.6125	17394.43	7969.94	
STD		2254.22	799.57		3146.77	780.65	
absolute mean		<b>11645.30</b>			<b>9424.49</b>		
absolute STD		<b>3053.78</b>			<b>3927.42</b>		
							<b>0.02</b>

	11_noDOX unstained	11_noDOX TMRM	11_noDOX TMRM_FCCP	11_DOX unstained	11_DOX TMRM	11_DOX TMRM_FCCP	p-value
EXP2							
15-Jul	2078.70	10833.45	5650.85	2087.52	9828.93	4774.42	
	2105.60	10877.40	3658.76	2050.34	9283.47	4580.04	
	2263.89	7682.76	4278.92	2367.12	7451.42	4159.02	
	2271.89	8735.14	4319.75	1997.36	6262.65	4498.02	
	2376.90	6069.11	3989.8	2429.62	6902.54	4505.16	
mean	2219.40	8839.57	4379.62	2186.392	7945.80	4503.33	
STD		2070.80	758.51		1541.21	222.46	
absolute mean		<b>4459.96</b>			<b>3442.47</b>		
absolute STD		<b>2829.31</b>			<b>1763.67</b>		
							<b>0.50</b>

	11_noDOX unstained	11_noDOX TMRM	11_noDOX TMRM_FCCP	11_DOX unstained	11_DOX TMRM	11_DOX TMRM_FCCP	p-value
EXP3							
16-Jul	1937.81	8184.4	4314.97	2029.65	8228.4	4004.75	
	2019.39	7971.00	3731.03	2036.15	6850.9	3934.88	
	2323.34	6402.66	3442.40	2414.76	6647.2	3199.21	
	2227.73	5633.61	4126.71	1787.53	3873.1	3285.96	
	2346.81	4017.2	2899.1	2176.34	5248.9	3263.51	
mean	2171.02	6441.77	3702.84	2088.886	6169.70	3537.66	
STD		1725.43	563.25		1662.27	396.55	
absolute mean		<b>2738.93</b>			<b>2632.04</b>		
absolute STD		<b>2288.68</b>			<b>2058.82</b>		
							<b>0.15</b>

## superoxide detection

Tab. 4: data for superoxide detection assays on MDCK-p30 cells

	p30_noDOX_noMS	p30_noDOX_MS	p30_DOX_noMS	p30_DOX_MS	p-value
EXP1					
10-May	971.31	1380.61	897.38	1618.20	
	943.87	1390.61	893.83	1608.84	
	925.84	1577.10	934.47	1625.82	
mean	947.01	1449.44	908.56	1617.62	
STD	22.90	133.57	22.51	31.01	
<b>absolute mean</b>		<b>502.43</b>		<b>709.06</b>	
<b>absolute STD</b>		<b>156.46</b>		<b>53.52</b>	
					<b>0.01</b>

	p30_noDOX_noMS	p30_noDOX_MS	p30_DOX_noMS	p30_DOX_MS	p-value
EXP2					
15-May	1195.86	1509.39	1049.91	1426.68	
	1169.02	1623.35	1163.42	1528.85	
	1166.08	1570.79	1177.18	1593.88	
	1186.01	1566.49	1178.84	1610.09	
	1187.36	1579.78	1184.85	1620.82	
mean	1180.87	1569.96	1150.84	1556.06	
STD	12.77	53.48	56.96	137.62	
<b>absolute mean</b>		<b>389.09</b>		<b>405.22</b>	
<b>absolute STD</b>		<b>66.25</b>		<b>194.59</b>	
					<b>0.25</b>

Tab. 5: data for superoxide detection assays on MDCK-p15 cells

	p15_noDOX_noMS	p15_noDOX_MS	p15_DOX_noMS	p15_DOX_MS	p-value
EXP1					
9-May	1941.69	3427.12	1369.29	2638.99	
	2087.51	3478.64	1425.30	2903.16	
	1943.14	3081.13	1208.13	2969.02	
mean	1990.78	3328.96	1334.24	2837.06	
STD	83.77	299.94	112.75	287.41	
<b>absolute mean</b>		<b>1338.18</b>		<b>1502.82</b>	
<b>absolute STD</b>		<b>383.72</b>		<b>400.16</b>	
					<b>0.17</b>

	p15_noDOX_noMS	p15_noDOX_MS	p15_DOX_noMS	p15_DOX_MS	p-value
EXP2					
19-May	1085.83	1570.09	983.99	1598.66	
	1046.45	1576.34	1062.19	1561.43	
	1090.67	1682.50	1014.22	1565.66	
	1011.25	1619.54	1049.34	1607.53	
	1079.93	1640.41	1025.55	1562.9	
mean	1062.83	1617.78	1027.06	1579.24	
STD	33.64	80.26	30.63	52.69	
<b>absolute mean</b>		<b>554.95</b>		<b>552.18</b>	
<b>absolute STD</b>		<b>113.90</b>		<b>83.32</b>	
					<b>0.45</b>

Tab. 6: data for superoxide detection assays on MDCK-II control cells

	II_noDOX_noMS	II_noDOX_MS	II_DOX_noMS	II_DOX_MS	p-value
EXP1					
12-May	951.09	1329.33	850.97	1311.94	
	961.30	1312.99	872.26	1297.63	
	963.24	1318.22	953.64	1358.52	
mean	958.54	1320.18	892.29	1322.70	
STD	6.53	14.87	54.19	86.02	
<b>absolute mean</b>		<b>361.64</b>		<b>430.41</b>	
<b>absolute STD</b>		<b>21.40</b>		<b>140.21</b>	
					<b>0.01</b>

	II_noDOX_noMS	II_noDOX_MS	II_DOX_noMS	II_DOX_MS	p-value
EXP2					
15-May	1026.96	1436.43	900.05	1346.15	
	1055.87	1425.31	924.91	1371.02	
	991.58	1419.21	893.67	1386.38	
	992.86	1403.62	879.7	1384.13	
	986.27	1467.93	922.17	1302.06	
mean	1010.708	1430.5	904.1	1357.948	
STD	29.94	53.99	19.24	54.33	
<b>absolute mean</b>		<b>419.79</b>		<b>453.85</b>	
<b>absolute STD</b>		<b>83.93</b>		<b>73.57</b>	
					<b>0.56</b>

## growth curves

Tab. 7: data for growth curve assay on MDCK-p30 cells in standard glucose

	1g/L glucose	cells/ $\mu$ l	cells/ $\mu$ l	cells total	cells total	p-value
$\Delta t$ in h	V in $\mu$ l	p30_noDOX	p30_DOX	p30_noDOX	p30_DOX	
0	500	27	30	13500	15000	
		28	30	14000	15000	
		28	30	14000	15000	
		26	28	13000	14000	
		26	31	13000	15500	
		29	32	14500	16000	
<b>mean</b>		<b>27</b>	<b>30</b>	<b>13667</b>	<b>15083</b>	
<b>STD</b>		<b>1.2</b>	<b>1.3</b>	<b>605.5</b>	<b>664.6</b>	
						<b>&lt;0.01</b>
24	1000	20	20	20000	20000	
		18	25	18000	25000	
		22	19	22000	19000	
		21	27	21000	27000	
		20	23	20000	23000	
		18	19	18000	19000	
<b>mean</b>		<b>20</b>	<b>22</b>	<b>19833</b>	<b>22167</b>	
<b>STD</b>		<b>1.6</b>	<b>3.4</b>	<b>1602.1</b>	<b>3371.4</b>	
						<b>0.08</b>
48	1000	88	76	88000	76000	
		55	53	55000	53000	
		48	58	48000	58000	
		52	54	52000	54000	
		46	60	46000	60000	
		53	68	53000	68000	
<b>mean</b>		<b>57</b>	<b>62</b>	<b>57000</b>	<b>61500</b>	
<b>STD</b>		<b>15.5</b>	<b>8.9</b>	<b>15543.5</b>	<b>8893.8</b>	
						<b>0.28</b>
72	1000	47	54	47000	54000	
		90	56	90000	56000	
		69	79	69000	79000	
		72	58	72000	58000	
		65	73	65000	73000	
		39	76	39000	76000	
<b>mean</b>		<b>64</b>	<b>66</b>	<b>63667</b>	<b>66000</b>	
<b>STD</b>		<b>18.3</b>	<b>11.2</b>	<b>18326.7</b>	<b>11189.3</b>	
						<b>0.40</b>

Tab. 8: data for growth curve assay on MDCK-p30 cells in standard glucose extension

120	1500	46	54	69000	81000	
		42	58	63000	87000	
		45	61	67500	91500	
		51	61	76500	91500	
		48	54	72000	81000	
		34	51	51000	76500	
<b>mean</b>		<b>44</b>	<b>57</b>	<b>66500</b>	<b>84750</b>	
<b>STD</b>		<b>5.9</b>	<b>4.1</b>	<b>8831.8</b>	<b>6202.8</b>	
						<b>&lt;0.001</b>
168	1500	35	29	52500.0	43500.0	
		47	41	70500.0	61500.0	
		48	35	72000.0	52500.0	
		49	41	73500.0	61500.0	
		50	43	75000.0	64500.0	
		45	35	67500.0	52500.0	
<b>mean</b>		<b>45.7</b>	<b>37.3</b>	<b>68500</b>	<b>56000</b>	
<b>STD</b>		<b>5.5</b>	<b>5.3</b>	<b>8252.3</b>	<b>7918.3</b>	
						<b>0.01</b>
216	1500	17	16	25500	24000	
		23	22	34500	33000	
		20	20	30000	30000	
		20	21	30000	31500	
		16	21	24000	31500	
		18	27	27000	40500	
<b>mean</b>		<b>19</b>	<b>21</b>	<b>28500</b>	<b>31750</b>	
<b>STD</b>		<b>2.5</b>	<b>3.5</b>	<b>3794.7</b>	<b>5317.4</b>	
						<b>0.13</b>

Tab. 9: data for growth curve assay on MDCK-II control cells for MDCK-p30 cells in standard glucose

	1g/L glucose	cells/ $\mu$ l	cells/ $\mu$ l	cells total	cells total	p-value
$\Delta t$ in h	V in $\mu$ l	II_noDOX	II_DOX	II_noDOX	II_DOX	
0	1000	17	18	17000	18000	
		18	18	18000	18000	
		19	19	19000	19000	
		19	19	19000	19000	
		19	18	19000	18000	
		21	20	21000	20000	
<b>mean</b>	<b>mean</b>	<b>19</b>	<b>19</b>	<b>18833</b>	<b>18667</b>	
<b>STD</b>	<b>STD</b>	<b>1.3</b>	<b>0.8</b>	<b>1329.2</b>	<b>816.5</b>	
						<b>0.40</b>
24	1000	49	47	49000	47000	
		43	44	43000	44000	
		46	36	46000	36000	
		45	34	45000	34000	
		45	42	45000	42000	
		42	39	42000	39000	
<b>mean</b>	<b>mean</b>	<b>45</b>	<b>40</b>	<b>45000</b>	<b>40333</b>	
<b>STD</b>	<b>STD</b>	<b>2.4</b>	<b>4.9</b>	<b>2449.5</b>	<b>4926.1</b>	
						<b>0.03</b>
48	1000	112	76	112000	76000	
		86	75	86000	75000	
		88	70	88000	70000	
		114	94	114000	94000	
		99	83	99000	83000	
		89	78	89000	78000	
<b>mean</b>		<b>98</b>	<b>79</b>	<b>98000</b>	<b>79333</b>	
<b>STD</b>		<b>12.5</b>	<b>8.3</b>	<b>12474.0</b>	<b>8334.7</b>	
						<b>&lt;0.01</b>
72	1500	63	55	94500	82500	
		65	61	97500	91500	
		86	59	129000	88500	
		75	63	112500	94500	
		59	58	88500	87000	
		63	51	94500	76500	
<b>mean</b>		<b>69</b>	<b>58</b>	<b>102750</b>	<b>86750</b>	
<b>STD</b>		<b>10.1</b>	<b>4.3</b>	<b>15171.5</b>	<b>6463.4</b>	
						<b>0.02</b>

Tab. 10: data for growth curve assay on MDCK-II control cells for MDCK-p30 cells in standard glucose extension

120	1500	81	76	121500	114000	
		69	78	103500	117000	
		95	71	142500	106500	
		87	56	130500	84000	
		93	52	139500	78000	
		71	74	106500	111000	
<b>mean</b>		<b>83</b>	<b>68</b>	<b>124000</b>	<b>101750</b>	
<b>STD</b>		<b>11.0</b>	<b>11.0</b>	<b>16477.3</b>	<b>16552.2</b>	
						<b>0.02</b>
168	1500	52	55	78000	82500	
		43	55	64500	82500	
		47	47	70500	70500	
		50	55	75000	82500	
		54	55	81000	82500	
		49	46	73500	69000	
<b>mean</b>		<b>49</b>	<b>52</b>	<b>73750</b>	<b>78250</b>	
<b>STD</b>		<b>3.9</b>	<b>4.4</b>	<b>5803.0</b>	<b>6601.1</b>	
						<b>0.12</b>
216	1500	15	14	22500	21000	
		38	26	57000	39000	
		46	24	69000	36000	
		40	39	60000	58500	
		34	22	51000	33000	
		34	27	51000	40500	
<b>mean</b>		<b>35</b>	<b>25</b>	<b>51750</b>	<b>38000</b>	
<b>STD</b>		<b>10.5</b>	<b>8.1</b>	<b>15810.6</b>	<b>12210.7</b>	
						<b>&lt;0.01</b>

Tab. 11: data for growth curve assay on MDCK-p30 cells in low glucose

	0.1g/L glucose	cells/ $\mu$ l	cells/ $\mu$ l	cells total	cells total	p-value
$\Delta t$ in h	V in $\mu$ l	p30_noDOX	p30_DOX	p30_noDOX	p30_DOX	
0	500	19	13	9500	6500	
		18	14	9000	7000	
		17	15	8500	7500	
		17	14	8500	7000	
		20	14	10000	7000	
		16	15	8000	7500	
<b>mean</b>		<b>18</b>	<b>14</b>	<b>8917</b>	<b>7083</b>	
<b>STD</b>		<b>1.5</b>	<b>0.8</b>	<b>736.0</b>	<b>376.4</b>	
						<b>&lt;0.001</b>
24	500	9	6	4500	3000	
		9	7	4500	3500	
		9	7	4500	3500	
		11	8	5500	4000	
		9	7	4500	3500	
		10	7	5000	3500	
<b>mean</b>		<b>10</b>	<b>7</b>	<b>4750</b>	<b>3500</b>	
<b>STD</b>		<b>0.8</b>	<b>0.6</b>	<b>418.3</b>	<b>316.2</b>	
						<b>&lt;0.001</b>
48	700	16	13	11200	9100	
		15	14	10500	9800	
		15	12	10500	8400	
		18	15	12600	10500	
		18	13	12600	9100	
		17	12	11900	8400	
<b>mean</b>		<b>17</b>	<b>13</b>	<b>11550</b>	<b>9217</b>	
<b>STD</b>		<b>1.4</b>	<b>1.2</b>	<b>964.9</b>	<b>818.3</b>	
						<b>&lt;0.01</b>
72	700	21	17	14700	11900	
		21	19	14700	13300	
		22	21	15400	14700	
		21	21	14700	14700	
		19	22	13300	15400	
		23	22	16100	15400	
<b>mean</b>		<b>21</b>	<b>20</b>	<b>14817</b>	<b>14233</b>	
<b>STD</b>		<b>1.3</b>	<b>2.0</b>	<b>930.4</b>	<b>1376.5</b>	
						<b>0.20</b>

Tab. 12: data for growth curve assay on MDCK-p30 cells in low glucose extension

96	700	24	19	16800	13300	
		22	25	15400	17500	
		22	19	15400	13300	
		19	16	13300	11200	
		16	20	11200	14000	
		20	16	14000	11200	
<b>mean</b>		<b>21</b>	<b>19</b>	<b>14350</b>	<b>13417</b>	
<b>STD</b>		<b>2.8</b>	<b>3.3</b>	<b>1967.5</b>	<b>2318.1</b>	
						<b>0.23</b>
144	700	15	13	10500	9100	
		20	19	14000	13300	
		13	19	9100	13300	
		13	15	9100	10500	
		16	16	11200	11200	
		14	16	9800	11200	
<b>mean</b>		<b>15.2</b>	<b>16.3</b>	<b>10617</b>	<b>11433</b>	
<b>STD</b>		<b>2.6</b>	<b>2.3</b>	<b>1847.6</b>	<b>1636.7</b>	
						<b>0.22</b>
192	500	7	7	3500	3500	
		8	10	4000	5000	
		8	6	4000	3000	
		8	7	4000	3500	
		8	11	4000	5500	
		9	9	4500	4500	
<b>mean</b>		<b>8</b>	<b>8</b>	<b>4000</b>	<b>4167</b>	
<b>STD</b>		<b>0.6</b>	<b>2.0</b>	<b>316.2</b>	<b>983.2</b>	
						<b>0.35</b>

Tab. 13: data for growth curve assay on MDCK-II control cells for MDCK-p30 cells in low glucose

	0.1g/L glucose	cells/ $\mu$ l	cells/ $\mu$ l	cells total	cells total	p-value
$\Delta$ t in h	V in $\mu$ l	II_noDOX	II_DOX	II_noDOX	II_DOX	
0	500	27	21	13500	10500	
		21	19	10500	9500	
		20	22	10000	11000	
		23	23	11500	11500	
		33	21	16500	10500	
		24	25	12000	12500	
<b>mean</b>	<b>mean</b>	<b>25</b>	<b>22</b>	<b>12333</b>	<b>10917</b>	
<b>STD</b>	<b>STD</b>	<b>4.8</b>	<b>2.0</b>	<b>2380.5</b>	<b>1020.6</b>	
						<b>0.10</b>
24	500	11	9	5500	4500	
		14	12	7000	6000	
		7	10	3500	5000	
		11	12	5500	6000	
		8	15	4000	7500	
		9	11	4500	5500	
<b>mean</b>	<b>mean</b>	<b>10</b>	<b>12</b>	<b>5000</b>	<b>5750</b>	
<b>STD</b>	<b>STD</b>	<b>2.5</b>	<b>2.1</b>	<b>1264.9</b>	<b>1036.8</b>	
						<b>0.14</b>
48	700	12	14	8400	9800	
		15	8	10500	5600	
		14	14	9800	9800	
		9	10	6300	7000	
		15	9	10500	6300	
		10	9	7000	6300	
<b>mean</b>		<b>13</b>	<b>11</b>	<b>8750</b>	<b>7467</b>	
<b>STD</b>		<b>2.6</b>	<b>2.7</b>	<b>1811.9</b>	<b>1860.8</b>	
						<b>0.13</b>
72	700	26	20	18200	14000	
		17	22	11900	15400	
		18	16	12600	11200	
		20	26	14000	18200	
		23	18	16100	12600	
		16	17	11200	11900	
<b>mean</b>		<b>20</b>	<b>20</b>	<b>14000</b>	<b>13883</b>	
<b>STD</b>		<b>3.8</b>	<b>3.7</b>	<b>2693.0</b>	<b>2597.2</b>	
						<b>0.47</b>

Tab. 14: data for growth curve assay on MDCK-II control cells for MDCK-p30 cells in low glucose extension

96	700	24	16	16800	11200	
		24	17	16800	11900	
		22	16	15400	11200	
		19	18	13300	12600	
		20	15	14000	10500	
		22	16	15400	11200	
<b>mean</b>		<b>22</b>	<b>16</b>	<b>15283</b>	<b>11433</b>	
<b>STD</b>		<b>2.0</b>	<b>1.0</b>	<b>1428.9</b>	<b>723.0</b>	
						<b>&lt;0.001</b>
144	700	15	14	10500	9800	
		18	17	12600	11900	
		15	17	10500	11900	
		13	15	9100	10500	
		18	19	12600	13300	
		13	12	9100	8400	
<b>mean</b>		<b>15</b>	<b>16</b>	<b>10733</b>	<b>10967</b>	
<b>STD</b>		<b>2.3</b>	<b>2.5</b>	<b>1575.6</b>	<b>1752.3</b>	
						<b>0.41</b>
192	500	9	11	4500	5500	
		6	9	3000	4500	
		5	7	2500	3500	
		6	5	3000	2500	
		6	9	3000	4500	
		8	9	4000	4500	
<b>mean</b>		<b>7</b>	<b>8</b>	<b>3333</b>	<b>4167</b>	
<b>STD</b>		<b>1.5</b>	<b>2.1</b>	<b>752.8</b>	<b>1032.8</b>	
						<b>0.07</b>

Tab. 15: data for growth curve assay on MDCK-p15 cells in standard glucose

	1g/L glucose	cells/ $\mu$ l	cells/ $\mu$ l	cells total	cells total	p-value
$\Delta t$ in h	V in $\mu$ l	p15_noDOX	p15_DOX	p15_noDOX	p15_DOX	
0	500	24	20	12000	10000	
		26	28	13000	14000	
		34	26	17000	13000	
		23	23	11500	11500	
		21	24	10500	12000	
		21	22	10500	11000	
<b>mean</b>		<b>25</b>	<b>24</b>	<b>12417</b>	<b>11917</b>	
<b>STD</b>		<b>4.9</b>	<b>2.9</b>	<b>2437.6</b>	<b>1428.9</b>	
						<b>0.34</b>
24	500	9	7	4500	3500	
		10	10	5000	5000	
		10	9	5000	4500	
		10	8	5000	4000	
		9	10	4500	5000	
		9	8	4500	4000	
<b>mean</b>		<b>10</b>	<b>9</b>	<b>4750</b>	<b>4333</b>	
<b>STD</b>		<b>0.5</b>	<b>1.2</b>	<b>273.9</b>	<b>605.5</b>	
						<b>0.08</b>
48	700	22	19	15400	13300	
		19	15	13300	10500	
		20	19	14000	13300	
		21	20	14700	14000	
		22	19	15400	13300	
		25	19	17500	13300	
<b>mean</b>		<b>22</b>	<b>19</b>	<b>15050</b>	<b>12950</b>	
<b>STD</b>		<b>2.1</b>	<b>1.8</b>	<b>1451.6</b>	<b>1232.5</b>	
						<b>0.01</b>
72	1000	35	34	35000	34000	
		40	35	40000	35000	
		31	30	31000	30000	
		37	32	37000	32000	
		36	30	36000	30000	
		36	42	36000	42000	
<b>mean</b>		<b>36</b>	<b>34</b>	<b>35833</b>	<b>33833</b>	
<b>STD</b>		<b>2.9</b>	<b>4.5</b>	<b>2926.9</b>	<b>4490.7</b>	
						<b>0.19</b>

Tab. 16: data for growth curve assay on MDCK-p15 cells in standard glucose extension

120	1500	47	26	70500	39000	
		59	45	88500	67500	
		54	52	81000	78000	
		62	52	93000	78000	
		46	46	69000	69000	
		42	45	63000	67500	
<b>mean</b>		<b>52</b>	<b>44</b>	<b>77500</b>	<b>66500</b>	
<b>STD</b>		<b>7.9</b>	<b>9.6</b>	<b>11874.3</b>	<b>14345.7</b>	
						<b>0.09</b>
144	1500	41.0	23.0	61500.0	34500.0	
		43.0	36.0	64500.0	54000.0	
		39.0	35.0	58500.0	52500.0	
		44.0	31.0	66000.0	46500.0	
		39.0	38.0	58500.0	57000.0	
		39.0	40.0	58500.0	60000.0	
<b>mean</b>		<b>40.8</b>	<b>33.8</b>	<b>61250</b>	<b>50750</b>	
<b>STD</b>		<b>2.2</b>	<b>6.1</b>	<b>3342.9</b>	<b>9169.2</b>	
						<b>0.01</b>
192	1000	25	8	25000	8000	
		21	9	21000	9000	
		25	11	25000	11000	
		17	14	17000	14000	
		21	11	21000	11000	
		16	11	16000	11000	
<b>mean</b>		<b>21</b>	<b>11</b>	<b>20833</b>	<b>10667</b>	
<b>STD</b>		<b>3.8</b>	<b>2.1</b>	<b>3816.6</b>	<b>2065.6</b>	
						<b>&lt;0.001</b>
240	1000	10	5	10000	5000	
		4	4	4000	4000	
		9	8	9000	8000	
		7	9	7000	9000	
		10	9	10000	9000	
		3	3	3000	3000	
<b>mean</b>		<b>7</b>	<b>6</b>	<b>7167</b>	<b>6333</b>	
<b>STD</b>		<b>3.1</b>	<b>2.7</b>	<b>3060.5</b>	<b>2658.3</b>	
						<b>0.31</b>

Tab. 17: data for growth curve assay on MDCK-II control cells for MDCK-p15 cells in standard glucose

	1g/L glucose	cells/ $\mu$ l	cells/ $\mu$ l	cells total	cells total	p-value
$\Delta t$ in h	V in $\mu$ l	II_noDOX	II_DOX	II_noDOX	II_DOX	
0	500	23	25	11500	12500	
		26	26	13000	13000	
		36	22	18000	11000	
		26	31	13000	15500	
		21	26	10500	13000	
		27	25	13500	12500	
<b>mean</b>	<b>mean</b>	<b>27</b>	<b>26</b>	<b>13250</b>	<b>12917</b>	
<b>STD</b>	<b>STD</b>	<b>5.2</b>	<b>2.9</b>	<b>2583.6</b>	<b>1463.4</b>	
						<b>0.40</b>
24		9	8	4500	4000	
		9	10	4500	5000	
		11	14	5500	7000	
		7	10	3500	5000	
		7	10	3500	5000	
		6	10	3000	5000	
<b>mean</b>	<b>mean</b>	<b>8</b>	<b>10</b>	<b>4083</b>	<b>5167</b>	
<b>STD</b>	<b>STD</b>	<b>1.8</b>	<b>2.0</b>	<b>917.4</b>	<b>983.2</b>	
						<b>0.04</b>
48	700	19	15	13300	10500	
		23	24	16100	16800	
		17	17	11900	11900	
		18	22	12600	15400	
		17	19	11900	13300	
		15	21	10500	14700	
<b>mean</b>		<b>18</b>	<b>20</b>	<b>12717</b>	<b>13767</b>	
<b>STD</b>		<b>2.7</b>	<b>3.3</b>	<b>1899.9</b>	<b>2328.7</b>	
						<b>0.21</b>
72	1000	37	44	37000	44000	
		39	39	39000	39000	
		28	28	28000	28000	
		54	40	54000	40000	
		34	35	34000	35000	
		36	30	36000	30000	
<b>mean</b>		<b>38</b>	<b>36</b>	<b>38000</b>	<b>36000</b>	
<b>STD</b>		<b>8.7</b>	<b>6.2</b>	<b>8694.8</b>	<b>6164.4</b>	
						<b>0.33</b>

Tab. 18: data for growth curve assay on MDCK-II control cells for MDCK-p15 cells in standard glucose extension

120	1000	86	57	86000	57000	
		104	78	104000	78000	
		71	84	71000	84000	
		89	90	89000	90000	
		93	83	93000	83000	
		90	73	90000	73000	
<b>mean</b>		<b>89</b>	<b>78</b>	<b>88833</b>	<b>77500</b>	
<b>STD</b>		<b>10.7</b>	<b>11.6</b>	<b>10722.3</b>	<b>11571.5</b>	
						<b>0.05</b>
144	1500	60	50	90000	75000	
		74	70	111000	105000	
		77	62	115500	93000	
		68	75	102000	112500	
		79	71	118500	106500	
		78	70	117000	105000	
<b>mean</b>		<b>73</b>	<b>66</b>	<b>109000</b>	<b>99500</b>	
<b>STD</b>		<b>7.4</b>	<b>9.0</b>	<b>11049.9</b>	<b>13572.0</b>	
						<b>0.11</b>
192	1000	22	25	22000	25000	
		47	55	47000	55000	
		51	75	51000	75000	
		54	72	54000	72000	
		41	61	41000	61000	
		40	68	40000	68000	
<b>mean</b>		<b>43</b>	<b>59</b>	<b>42500</b>	<b>59333</b>	
<b>STD</b>		<b>11.4</b>	<b>18.3</b>	<b>11432.4</b>	<b>18337.6</b>	
						<b>0.04</b>
240	500	16.0	18.0	8000.0	9000.0	
		35.0	38.0	17500.0	19000.0	
		23.0	16.0	11500.0	8000.0	
		42.0	35.0	21000.0	17500.0	
		28.0	31.0	14000.0	15500.0	
		34.0	33.0	17000.0	16500.0	
<b>mean</b>		<b>29.7</b>	<b>28.5</b>	<b>14833.3</b>	<b>14250.0</b>	
<b>STD</b>		<b>9.3</b>	<b>9.2</b>	<b>4654.7</b>	<b>4612.5</b>	
						<b>0.42</b>

Tab. 19: data for growth curve assay on MDCK-p15 cells in low glucose

	0.1g/L glucose	cells/ $\mu$ l	cells/ $\mu$ l	incl. dilution factor	incl. dilution factor	p-value
$\Delta t$ in h	V in $\mu$ l	p15_noDOX	p15_DOX	p15_noDOX	p15_DOX	
0	500	29	22	14500	11000	
		24	26	12000	13000	
		29	28	14500	14000	
		28	31	14000	15500	
		26	29	13000	14500	
		33	30	16500	15000	
<b>mean</b>		<b>28</b>	<b>28</b>	<b>14083</b>	<b>13833</b>	
<b>STD</b>		<b>3.1</b>	<b>3.3</b>	<b>1530.3</b>	<b>1633.0</b>	
						<b>0.39</b>
22	500	8	7	4000	3500	
		9	6	4500	3000	
		7	7	3500	3500	
		7	7	3500	3500	
		6	8	3000	4000	
		7	8	3500	4000	
<b>mean</b>		<b>7</b>	<b>7</b>	<b>3667</b>	<b>3583</b>	
<b>STD</b>		<b>1.0</b>	<b>0.8</b>	<b>516.4</b>	<b>376.4</b>	
						<b>0.38</b>
48	500	19	17	9500	8500	
		20	18	10000	9000	
		24	15	12000	7500	
		23	17	11500	8500	
		23	17	11500	8500	
		21	18	10500	9000	
<b>mean</b>		<b>22</b>	<b>17</b>	<b>10833</b>	<b>8500</b>	
<b>STD</b>		<b>2.0</b>	<b>1.1</b>	<b>983.2</b>	<b>547.7</b>	
						<b>&lt;0.001</b>
75	1000	22	16	22000	16000	
		18	18	18000	18000	
		20	16	20000	16000	
		23	14	23000	14000	
		24	19	24000	19000	
		24	20	24000	20000	
<b>mean</b>		<b>22</b>	<b>17</b>	<b>21833</b>	<b>17167</b>	
<b>STD</b>		<b>2.4</b>	<b>2.2</b>	<b>2401.4</b>	<b>2228.6</b>	
						<b>&lt;0.01</b>

Tab. 20: data for growth curve assay on MDCK-p15 cells in low glucose extension

102	1200	28	18	33600	21600	
		23	19	27600	22800	
		22	16	26400	19200	
		21	19	25200	22800	
		18	19	21600	22800	
		20	19	24000	22800	
<b>mean</b>		<b>22</b>	<b>18</b>	<b>26400</b>	<b>22000</b>	
<b>STD</b>		<b>3.4</b>	<b>1.2</b>	<b>4087.1</b>	<b>1453.3</b>	
						<b>0.02</b>
119	1200	20.0	19.0	24000.0	22800.0	
		23.0	20.0	27600.0	24000.0	
		22.0	19.0	26400.0	22800.0	
		21.0	18.0	25200.0	21600.0	
		24.0	22.0	28800.0	26400.0	
		18.0	20.0	21600.0	24000.0	
<b>mean</b>		<b>21.3</b>	<b>19.7</b>	<b>25600</b>	<b>23600</b>	
<b>STD</b>		<b>2.2</b>	<b>1.4</b>	<b>2592.3</b>	<b>1639.5</b>	
						<b>0.07</b>
<b>167</b>	1200	11	10	13200	12000	
		13	13	15600	15600	
		11	13	13200	15600	
		9	13	10800	15600	
		12	10	14400	12000	
		8	9	9600	10800	
<b>mean</b>		<b>11</b>	<b>11</b>	<b>12800</b>	<b>13600</b>	
<b>STD</b>		<b>1.9</b>	<b>1.9</b>	<b>2234.3</b>	<b>2234.3</b>	
						<b>0.27</b>

Tab. 21: data for growth curve assay on MDCK-II control cells for MDCK-p15 cells in low glucose

	0.1g/L glucose	cells/ $\mu$ l	cells/ $\mu$ l	cells total	cells total	p-value
$\Delta t$ in h	V in $\mu$ l	II_noDOX	II_DOX	II_noDOX	II_DOX	
0	500	39	38	19500	19000	
		36	42	18000	21000	
		31	44	15500	22000	
		33	45	16500	22500	
		31	49	15500	24500	
		41	43	20500	21500	
<b>mean</b>	<b>mean</b>	<b>35</b>	<b>44</b>	<b>17583</b>	<b>21750</b>	
<b>STD</b>	<b>STD</b>	<b>4.2</b>	<b>3.6</b>	<b>2107.5</b>	<b>1809.7</b>	
						<b>&lt;0.01</b>
22	500	14	12	7000	6000	
		12	12	6000	6000	
		9	9	4500	4500	
		12	15	6000	7500	
		13	14	6500	7000	
		11	13	5500	6500	
<b>mean</b>	<b>mean</b>	<b>12</b>	<b>13</b>	<b>5917</b>	<b>6250</b>	
<b>STD</b>	<b>STD</b>	<b>1.7</b>	<b>2.1</b>	<b>861.2</b>	<b>1036.8</b>	
						<b>0.28</b>
48	500	17	14	8500	7000	
		11	13	5500	6500	
		10	11	5000	5500	
		15	14	7500	7000	
		13	14	6500	7000	
		13	16	6500	8000	
<b>mean</b>		<b>13</b>	<b>14</b>	<b>6583</b>	<b>6833</b>	
<b>STD</b>		<b>2.6</b>	<b>1.6</b>	<b>1281.3</b>	<b>816.5</b>	
						<b>0.35</b>
75	1000	27	30	27000	30000	
		23	23	23000	23000	
		23	26	23000	26000	
		19	21	19000	21000	
		24	33	24000	33000	
		23	26	23000	26000	
<b>mean</b>		<b>23</b>	<b>27</b>	<b>23167</b>	<b>26500</b>	
<b>STD</b>		<b>2.6</b>	<b>4.4</b>	<b>2562.6</b>	<b>4415.9</b>	
						<b>0.07</b>

Tab. 22: data for growth curve assay on MDCK-II control cells for MDCK-p15 cells in low glucose extension

102	1200	22	24	26400	28800	
		27	29	32400	34800	
		24	24	28800	28800	
		26	29	31200	34800	
		31	27	37200	32400	
		21	26	25200	31200	
<b>mean</b>		<b>25</b>	<b>27</b>	<b>30200</b>	<b>31800</b>	
<b>STD</b>		<b>3.7</b>	<b>2.3</b>	<b>4387.3</b>	<b>2710.0</b>	
						<b>0.23</b>
119	1200	15	13	18000	15600	
		20	18	24000	21600	
		17	13	20400	15600	
		21	18	25200	21600	
		18	21	21600	25200	
		14	25	16800	30000	
<b>mean</b>		<b>18</b>	<b>18</b>	<b>21000</b>	<b>21600</b>	
<b>STD</b>		<b>2.7</b>	<b>4.6</b>	<b>3286.3</b>	<b>5577.1</b>	
						<b>0.41</b>
<b>167</b>	1200	13	14	15600	16800	
		8	11	9600	13200	
		11	10	13200	12000	
		13	10	15600	12000	
		12	9	14400	10800	
		14	9	16800	10800	
<b>mean</b>		<b>12</b>	<b>11</b>	<b>14200</b>	<b>12600</b>	
<b>STD</b>		<b>2.1</b>	<b>1.9</b>	<b>2564.4</b>	<b>2245.0</b>	
						<b>0.14</b>

## cell permeabilization

Tab. 23: data for cell permeabilization assay on MDCK-p30 cells in standard glucose

t	p30_noDOX unstained in %	p30_noDOX stained in %	p30_DOX unstained in %	p30_DOX stained in %	p-value
0	0.0	12.0	0.1	14.1	
	0.0	15.3	0.0	14.0	
	0.1	10.7	0.0	13.4	
mean	<b>0.0</b>	<b>12.7</b>	<b>0.0</b>	<b>13.8</b>	0.22
24h	0.1	9.3	0.0	9.0	
	0.0	9.1	0.1	16.3	
	0.1	8.3	0.2	15.7	
mean	<b>0.1</b>	<b>8.9</b>	<b>0.1</b>	<b>13.7</b>	0.06
48h	0.0	8.0	0.0	7.7	
	0.0	9.8	0.3	10.2	
	0.0	9.6	0.1	9.5	
mean	<b>0.0</b>	<b>9.1</b>	<b>0.1</b>	<b>9.1</b>	0.50
72h	0.0	7.4	0.0	3.3	
	0.0	1.8	0.0	1.5	
	0.0	1.9	0.0	0.7	
mean	<b>0.0</b>	<b>3.7</b>	<b>0.0</b>	<b>1.8</b>	0.20
120h	0.0	5.8	0.0	2.7	
	0.0	4.6	0.0	3.9	
	0.0	6.3	0.0	5.4	
mean	<b>0.0</b>	<b>5.6</b>	<b>0.0</b>	<b>4.0</b>	0.08
168h	0.0	5.9	0.0	5.7	
	0.0	6.1	0.0	6.9	
	0.0	5.0	0.0	7.3	
mean	<b>0.0</b>	<b>5.7</b>	<b>0.0</b>	<b>6.6</b>	0.09
216h	0.0	10.8	0.4	10.5	
	0.3	15.0	0.3	11.4	
	0.1	16.0	0.2	8.3	
mean	<b>0.1</b>	<b>13.9</b>	<b>0.3</b>	<b>10.1</b>	0.05

Tab. 24: data for cell permeabilization assay on MDCK-II control cells for MDCK-p30 cells in standard glucose

	11_noDOX unstained in %	11_noDOX stained in %	11_DOX unstained in %	11_DOX stained in %	p-value
0h	0.2	7.6	0.1	8.6	
	0.2	13.0	0.2	9.6	
	0.3	8.1	0.0	5.5	
mean	<b>0.2</b>	<b>9.6</b>	<b>0.1</b>	<b>7.9</b>	0.24
24h	0.0	5.9	0.0	8.3	
	0.0	8.4	0.1	10.4	
	0.1	11.4	0.0	10.7	
mean	<b>0.0</b>	<b>8.6</b>	<b>0.0</b>	<b>9.8</b>	0.26
48h	0.0	7.1	0.2	8.2	
	0.0	7.9	0.0	8.3	
	0.0	6.6	0.0	6.9	
mean	<b>0.0</b>	<b>7.2</b>	<b>0.1</b>	<b>7.8</b>	0.18
72h	0.0	9.0	0.0	6.4	
	0.0	9.8	0.1	11.9	
	0.0	7.4	0.0	9.4	
mean	<b>0.0</b>	<b>8.7</b>	<b>0.0</b>	<b>9.2</b>	0.39
120h	0.0	6.8	0.0	5.4	
	0.0	5.2	0.0	6.0	
	0.0	4.3	0.0	4.6	
mean	<b>0.0</b>	<b>5.4</b>	<b>0.0</b>	<b>5.3</b>	0.46
168h	0.0	3.1	0.0	3.2	
	0.0	5.2	0.0	2.8	
	0.1	5.6	0.1	4.6	
mean	<b>0.0</b>	<b>4.6</b>	<b>0.0</b>	<b>3.5</b>	0.16
216h	0.0	6.7	0.0	5.1	
	0.1	8.0	0.1	10.5	
	0.1	6.6	0.1	9.7	
	<b>0.1</b>	<b>7.1</b>	<b>0.1</b>	<b>8.4</b>	0.24

Tab. 25: data for cell permeabilization assay on MDCK-p30 cells in low glucose

	p30_noDOX unstained in %	p30_noDOX stained in %	p30_DOX unstained in %	p30_DOX stained in %	p-value
0h	0.0	9.2	0.0	10.0	
	0.0	6.8	0.1	14.7	
	0.1	10.8	0.0	16.6	
mean	<b>0.0</b>	<b>8.9</b>	<b>0.0</b>	<b>13.8</b>	0.05
24h	0.0	13.6	0.0	15.9	
	0.0	16.9	0.0	25.7	
	0.2	15.6	0.5	23.8	
mean	<b>0.1</b>	<b>15.4</b>	<b>0.2</b>	<b>21.8</b>	0.06
48h	0.0	9.8	0.0	12.9	
	0.0	11.6	0.0	14.4	
	0.1	12.3	0.0	16.9	
mean	<b>0.0</b>	<b>11.2</b>	<b>0.0</b>	<b>14.7</b>	0.03
72h	0.0	5.5	0.0	8.9	
	0.0	10.5	0.1	8.1	
	0.0	9.6	0.1	9.7	
mean	<b>0.0</b>	<b>8.5</b>	<b>0.1</b>	<b>8.9</b>	0.42
96h	0.0	6.0	0.1	6.0	
	0.1	6.5	0.1	5.9	
	0.2	7.5	0.0	8.7	
mean	<b>0.1</b>	<b>6.7</b>	<b>0.1</b>	<b>6.9</b>	0.43
144h	0.2	8.6	0.0	8.9	
	0.2	9.6	0.1	7.7	
	0.2	7.4	0.2	7.8	
mean	<b>0.2</b>	<b>8.5</b>	<b>0.1</b>	<b>8.1</b>	0.31
192h	0.3	23.4	0.0	16.1	
	0.5	20.9	0.0	12.7	
	0.0	17.2	0.0	17.9	
mean	<b>0.3</b>	<b>20.5</b>	<b>0.0</b>	<b>15.6</b>	0.05

Tab. 26: data for cell permeabilization assay on MDCK-II control cells for MDCK-p30 cells in low glucose

	11_noDOX unstained in %	11_noDOX stained in %	11_DOX unstained in %	11_DOX stained in %	p-value
0h	0.0	14.4	0.1	9.4	
	0.0	12.7	0.0	6.6	
	0.0	13.4	0.0	8.2	
mean	<b>0.0</b>	<b>13.5</b>	<b>0.0</b>	<b>8.1</b>	0.002
24h	0.0	14.1	0.0	11.6	
	0.3	12.3	0.0	3.6	
	0.0	28.4	0.0	25.9	
mean	<b>0.1</b>	<b>18.3</b>	<b>0.0</b>	<b>13.7</b>	0.31
48h	0.0	12.4	0.0	16.3	
	0.0	16.2	0.0	15.5	
	0.1	15.1	0.0	15.6	
mean	<b>0.0</b>	<b>14.6</b>	<b>0.0</b>	<b>15.8</b>	0.17
72h	0.0	6.4	0.0	6.7	
	0.0	5.4	0.0	4.4	
	0.0	3.3	0.0	6.3	
mean	<b>0.0</b>	<b>5.0</b>	<b>0.0</b>	<b>5.8</b>	0.27
96h	0.1	3.8	0.0	3.3	
	0.2	5.4	0.0	6.1	
	0.0	6.5	0.1	4.6	
mean	<b>0.1</b>	<b>5.2</b>	<b>0.0</b>	<b>4.7</b>	0.32
144h	0.1	4.8	0.1	4.2	
	0.0	4.1	0.0	3.7	
	0.0	6.9	0.0	9.6	
mean	<b>0.0</b>	<b>5.3</b>	<b>0.0</b>	<b>5.8</b>	0.40
192h	0.0	18.3	0.0	25.0	
	0.0	21.9	0.2	17.8	
	0.4	26.2	0.0	28.0	
mean	<b>0.1</b>	<b>22.1</b>	<b>0.1</b>	<b>23.6</b>	0.36

Tab. 27: data for cell permeabilization assay on MDCK-p15 cells in standard glucose

	p15_noDOX unstained in %	p15_noDOX stained in %	p15_DOX unstained in %	p15_DOX stained in %	p-value
0h	0.0	20.9	0.0	12.6	
	0.0	11.8	0.0	17.1	
	0.1	15.5	0.0	21.8	
mean	<b>0.0</b>	<b>16.1</b>	<b>0.0</b>	<b>17.2</b>	0.39
24h	0.0	15.2	0.0	11.7	
	0.0	17.2	0.0	10.6	
	0.0	9.0	0.0	15.7	
mean	<b>0.0</b>	<b>13.8</b>	<b>0.0</b>	<b>12.7</b>	0.36
48h	0.0	12.1	0.1	13.3	
	0.0	12.0	0.1	15.1	
	0.0	9.3	0.1	15.2	
mean	<b>0.0</b>	<b>11.1</b>	<b>0.1</b>	<b>14.5</b>	0.02
72h	0.0	8.1	0.1	9.8	
	0.0	11.8	0.0	11.6	
	0.0	11.3	0.1	11.8	
mean	<b>0.0</b>	<b>10.4</b>	<b>0.1</b>	<b>11.1</b>	0.32
120h	0.0	2.9	0.0	2.4	
	0.0	4.0	0.0	3.1	
	0.0	5.8	0.0	2.6	
mean	<b>0.0</b>	<b>4.2</b>	<b>0.0</b>	<b>2.7</b>	0.08
144	0.0	3.8	0.1	3.0	
	0.0	4.2	0.0	4.1	
	0.0	4.8	0.0	3.8	
mean	<b>0.0</b>	<b>4.3</b>	<b>0.0</b>	<b>3.6</b>	0.11
192	0.0	10.7	0.0	8.3	
	0.1	10.6	0.0	14.4	
	0.1	10.4	0.1	11.2	
mean	<b>0.1</b>	<b>10.6</b>	<b>0.0</b>	<b>11.3</b>	0.35
240	0.0	15.6	0.0	15.2	
	0.2	9.9	0.0	12.3	
	0.4	24.5	0.4	23.9	
mean	<b>0.2</b>	<b>16.7</b>	<b>0.1</b>	<b>17.1</b>	0.47

Tab. 28: data for cell permeabilization assay on MDCK-II control cells for MDCK-p15 cells in standard glucose

	11_noDOX unstained in %	11_noDOX stained in %	11_DOX unstained in %	11_DOX stained in %	p-value
0h	0.0	13.7	0.0	9.7	
	0.0	7.0	0.1	8.3	
	0.1	12.0	0.1	7.8	
mean	<b>0.0</b>	<b>10.9</b>	<b>0.1</b>	<b>8.6</b>	0.17
24h	0.0	19.2	0.3	16.2	
	0.0	20.0	0.0	22.4	
	0.0	18.7	0.1	22.3	
mean	<b>0.0</b>	<b>19.3</b>	<b>0.1</b>	<b>20.3</b>	0.33
48h	0.0	15.7	0.0	15.6	
	0.1	17.3	0.0	16.6	
	0.2	15.0	0.1	16.9	
mean	<b>0.1</b>	<b>16.0</b>	<b>0.0</b>	<b>16.4</b>	0.33
72h	0.0	8.6	0.0	7.6	
	0.0	10.2	0.1	10.4	
	0.1	12.4	0.1	11.1	
mean	<b>0.0</b>	<b>10.4</b>	<b>0.1</b>	<b>9.7</b>	0.34
120h	0.0	2.5	0.0	3.0	
	0.1	2.3	0.0	3.5	
	0.1	2.6	0.0	3.1	
mean	<b>0.1</b>	<b>2.5</b>	<b>0.0</b>	<b>3.2</b>	0.007
144h	0.0	3.3	0.0	3.6	
	0.0	3.6	0.2	2.9	
	0.0	4.9	0.2	4.5	
mean	<b>0.0</b>	<b>3.9</b>	<b>0.1</b>	<b>3.7</b>	0.36
192h	0.0	4.6	0.0	3.0	
	0.0	6.8	0.0	4.1	
	0.0	6.8	0.0	4.5	
mean	<b>0.0</b>	<b>6.1</b>	<b>0.0</b>	<b>3.9</b>	0.03
240h	0.4	6.2	0.0	8.7	
	0.1	14.3	0.1	10.3	
	0.0	6.7	0.0	7.4	
mean	<b>0.2</b>	<b>9.1</b>	<b>0.0</b>	<b>8.8</b>	0.47

Tab. 29: data for cell permeabilization assay on MDCK-p15 cells in low glucose

	p15_noDOX unstained in %	p15_noDOX stained in %	p15_DOX unstained in %	p15_DOX stained in %	p-value
0h	0.0	3.5	0.0	2.5	
	0.0	2.0	0.0	1.9	
	0.0	1.9	0.1	1.5	
mean	<b>0.0</b>	<b>2.5</b>	<b>0.0</b>	<b>2.0</b>	0.22
22h	0.0	6.5	0.0	8.4	
	0.0	2.5	0.0	2.5	
	0.0	2.1	0.0	1.9	
mean	<b>0.0</b>	<b>3.7</b>	<b>0.0</b>	<b>4.3</b>	0.42
48h	0.0	8.4	0.0	11.2	
	0.0	6.0	0.0	7.2	
	0.1	3.3	0.2	10.2	
mean	<b>0.0</b>	<b>5.9</b>	<b>0.1</b>	<b>9.5</b>	0.06
75h	0.0	0.9	0.0	1.1	
	0.0	1.0	0.1	1.8	
	0.0	1.1	0.0	1.3	
mean	<b>0.0</b>	<b>1.0</b>	<b>0.0</b>	<b>1.4</b>	0.07
102h	0.2	4.8	0.0	2.1	
	0.0	4.2	0.0	4.3	
	0.0	6.5	0.0	2.9	
mean	<b>0.1</b>	<b>5.2</b>	<b>0.0</b>	<b>3.1</b>	0.06
119h	0.0	3.1	0.0	4.9	
	0.0	3.3	0.1	4.2	
	0.0	5.8	0.0	4.1	
mean	<b>0.0</b>	<b>4.1</b>	<b>0.0</b>	<b>4.4</b>	0.37
167h	0.0	12.3	0.0	10.9	
	0.0	8.4	0.0	11.5	
	0.0	9.8	0.2	10.6	
mean	<b>0.0</b>	<b>10.2</b>	<b>0.1</b>	<b>11.0</b>	0.26

Tab. 30: data for cell permeabilization assay on MDCK-II control cells for MDCK-p15 cells in low glucose

	11_noDOX unstained in %	11_noDOX stained in %	11_DOX unstained in %	11_DOX stained in %	p-value
0h	0.0	4.8	0.0	3.5	
	0.1	4.7	0.0	6.0	
	0.1	5.2	0.0	4.2	
mean	<b>0.1</b>	<b>4.9</b>	<b>0.0</b>	<b>4.6</b>	0.34
22h	0.0	6.8	0.0	4.0	
	0.0	5.1	0.0	4.3	
	0.0	4.5	0.2	3.5	
mean	<b>0.0</b>	<b>5.5</b>	<b>0.1</b>	<b>3.9</b>	0.05
48h	0.0	12.5	0.0	9.4	
	0.0	8.0	0.2	10.1	
	0.0	6.7	0.0	15.6	
mean	<b>0.0</b>	<b>9.1</b>	<b>0.1</b>	<b>11.7</b>	0.19
75h	0.0	1.8	0.0	1.5	
	0.0	1.4	0.0	1.6	
	0.0	2.0	0.0	2.3	
mean	<b>0.0</b>	<b>1.7</b>	<b>0.0</b>	<b>1.8</b>	0.42
102h	0.0	1.5	0.0	2.2	
	0.0	1.5	0.0	2.4	
	0.0	2.4	0.1	2.7	
mean	<b>0.0</b>	<b>1.8</b>	<b>0.0</b>	<b>2.4</b>	0.07
119h	0.0	1.5	0.0	3.4	
	0.0	2.7	0.0	4.3	
	0.0	3.7	0.0	5.4	
mean	<b>0.0</b>	<b>2.6</b>	<b>0.0</b>	<b>4.4</b>	0.06
167h	0.0	9.5	0.0	10.3	
	0.3	13.2	0.0	16.2	
	0.0	8.5	0.2	17.0	
mean	<b>0.1</b>	<b>10.4</b>	<b>0.1</b>	<b>14.5</b>	0.09